BL4B

Electronic Structure of DNA Characterized by Resonant Photoemission Spectroscopy

H. S. Kato[1], M. Furukawa[1], M. Kawai[1], M. Taniguchi[1,2], T. Kawai[1,2], T. Hatsui[3], N. Kosugi[3]

[1]*RIKEN (The Institute of Physical and Chemical Research), Wako 351-0198 Japan*
[2]*Institute of Scientific and Industrial Research, Osaka University, Ibaraki 567-0047 Japan*
[3]*Institute for Molecular Science, Okazaki 444-8585 Japan*

The characterization of electronic states near Fermi level of DNA duplexes has been desired to clarify the mechanisms of long-range charge migration in DNA, from the viewpoint of not only biochemistry but also molecular device materialization. Thorough stacking orbitals of DNA bases (Fig. 1), the dc conductivity model of DNA strands was proposed, over four decades ago, on the basis of electric conductivity measurements and a striking resemblance to conductive one-dimensional aromatic crystals. With the recent progress in nanotechnology, in addition, the electric conductivity of DNA has directly been measured in molecular scale. However, these characterizations of the electric property are still indefinite, and there is no significant observation on the electronic states near Fermi level of DNA for understanding of the charge migration mechanism. In this study, therefore, we carried out resonant photoemission spectroscopy (RPES) experiments near the Fermi level for both poly(dG)·poly(dC) (GC) and poly(dA)·poly(dT) (AT) DNA duplexes [1]. Since N atoms are included in only bases in DNA duplexes, the RPE spectra were obtained via the resonance from N 1*s* to unoccupied states, and thus we could purely extract the electronic orbital features of the bases in DNA.

Fig. 1 Schematic structure of a DNA double helix.

Experimental

Experiments were performed at the beamline BL4B of the UVSOR facility, in which the end-station (ultrahigh vacuum systems) is equipped with an electron energy analyzer (Scienta SES200) and a retarding-field electron detector for X-ray absorption spectroscopy (XAS). The obtained RPE intensities were normalized by the excitation light intensity monitored as mesh current. We prepared thick GC- and AT-DNA films on SiO_2/*p*-Si(111) substrates in the atmosphere. The film thickness prepared was estimated to be 100 - 200 nm. Comparing our observed Raman spectra [2] to those previously reported, we confirmed that DNA in the prepared thick films forms a mixture of A- and B-form double helixes. These samples were introduced into the ultrahigh vacuum via a sample entry system from the atmosphere, without baking procedures. Special care of freshness of DNA samples was taken throughout the experiments, to avoid any chemical changes. At the experiments, the sample was frequently replaced with new one, at least twice a day. This procedure also excluded accumulation of X-ray radiation damages on the surface. We confirmed suitable N 1s photoelectron spectra [2] for each sample.

Results and Discussion

An N *K*-edge XA spectrum of GC DNA is shown in the inset of Fig. 2. In the XA spectrum, two 1*s* - π* resonant peaks at 399.7 eV and 401.9 eV and a broad 1*s* - σ* resonant peak at 407 eV were observed. The off- and on-RPE spectra near the Fermi level of GC DNA are shown in Fig. 2 as a function of kinetic energy. The RPE spectra were measured at each resonant absorption peak marked on the XA spectrum shown in the inset. On the comparison to the off-RPE (normal Auger) spectrum, the on-RPE (resonant Auger) spectra are obviously involving additional components which is attributed to the N-*KLL* Auger electrons.

The resonant Auger signals could be extracted from the on-RPE spectra by subtracting the off-RPE spectra in binding energy plots, as the dotted lines in Fig. 2. The differential spectra commonly show a broad bump. Normally, the Auger electrons keep an identical distribution in kinetic energy, independently of excitation photon energies. The obtained resonant Auger signals were, however, strongly affected by

excitation energy; the lower photon energy light provides a higher kinetic energy distribution. This indicates that the excited electrons locate in the unoccupied states for, at least, a time scale of resonant Auger transition and affect its final state of the transition.

In addition, an appended component was observed at the first π* resonance, as marked by a dagger in Fig. 2. We attribute the additional component to that of participant Auger transition. This finding again indicates that the excited electrons locate in the π* states for, at least, the time scale of Auger transition.

In the case of the molecules chemisorbed on metals, such as CO/metals, their RPE spectra do not show the drastic peak shift of Auger electrons in kinetic energy. These are explained as that the molecular orbitals rehybridized with metal electronic states are delocalized, and the excited electrons in the chemisorbed molecules diffuse into the metal, immediately. In contrast, all features of the observed RPE spectra of DNA, as mentioned above, clearly show that the excited electron is localized at the excited orbitals. In other words, the unoccupied states of the bases in DNA duplexes are not delocalized.

The degree of the localization of excited electrons can be determined from the peak shift of resonant Auger signals, according to the report of Takata *et al.* [3]. For Ni metal, the *LMM* Auger peaks show a constant kinetic energy, *i.e.*, normal Auger transition behavior, under excitation above the photoabsorption maximum. For the $K_2Ni(CN)_4$ ionic crystal in which the $Ni(CN)_4$ complex exists as a quasi-isolated ion, on the other hand, the Ni-*LMM* Auger peaks show a downward shift as a function of photon energy with the slope of $\Delta KE/\Delta h\nu$ = -0.55 ± 0.05. For the vaporized Ca atom [4], the slope of a resonant Auger peak has been estimated to be -1, which would be the lower limit because of the condition ideally isolated. The upper limit must be zero as results at the Ni metal. In the case of DNA, the slope was estimated to be -0.5 ± 0.2 from the Auger peak shift shown in Fig. 1C. It is concluded that the degree of the localization of excited electrons at DNA bases is similar to that at the Ni complex in the ionic crystal.

Regarding electron migration mechanisms in DNA duplexes, several models have been proposed. Porath *et al*. carried out the conductivity measurements of a single GC DNA and described two antithetical models, namely, the charge hopping model between localized states and the charge transfer model through delocalized states [5]. They finally proposed that the charge transfer model is adequate on the basis of the observed voltage gap in I-V curves, although direct evidence could not be obtained. Our results, in contrast, clearly show the feature of the localized unoccupied orbitals of the bases in DNA. We hence conclude that the hopping model for electric conduction is pertinent when the electrons pass through the unoccupied states of bases.

Finally, we collate our results with recent biochemical research on charge migration in DNA duplexes. In relation to the biochemical aspects of DNA damage and repair, the charge migration mechanisms in DNA duplexes have been extensively discussed. In these arguments, the carrier is regarded as a hole formed by oxidation and migrates through the bases in DNA duplexes. In spite of the detailed analysis of the LUMO structure described above, the HOMO structure cannot be directly revealed by RPES. However, it is generally expected that the energetically deeper orbitals are more compact than the shallow ones. Hence, the observation of the localized LUMO suggests the localized HOMO in DNA, which is consistent with recent findings; for the long-range charge migration, the hole hopping model between the localized DNA-base orbitals with short tunneling has been inferred.

In summary, we characterized the electronic structure near Fermi level of DNA duplexes using RPES, in order to specify the charge migration mechanism. On RPES, we observed the kinetic energy shift of N-*KLL* resonant Auger electrons and the intensity enhancement of valence electrons for both GC and AT DNAs. These directly indicate the localized unoccupied orbitals of the bases. Hence, we conclude that the charge hopping model is suitable for electric conduction in DNA duplexes rather than the charge transfer model via delocalized states, when electrons pass through the π* states of DNA bases.

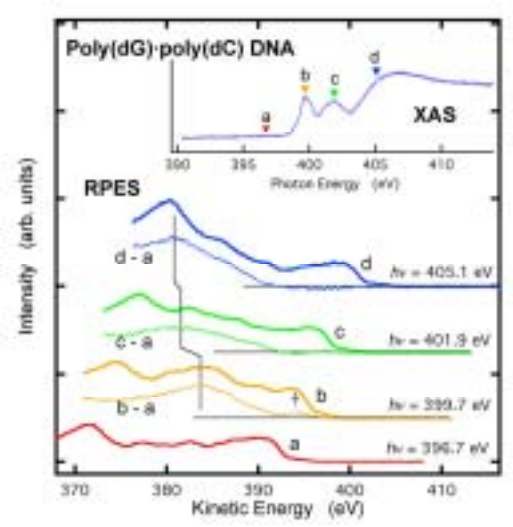

Fig. 2 Off- and on-RPE spectra of GC DNA. The inset shows an N *K*-edge X-ray absorption spectrum.

[1] H. S. Kato, M. Furukawa, M. Kawai, M. Taniguchi, T. Kawai, T. Hatsui, and N. Kosugi, Phys. Rev. Lett. **93** (2004) 086403.
[2] M. Furukawa *et al.*, (*to be published*).
[3] Y. Takata, T. Hatsui, and N. Kosugi, J. Electron Spectrosc. Relat. Phenom. **101-103** (1999) 443.
[4] K. Ueda *et al.*, Phys. Rev. A **54** (1996) 490.
[5] D. Porath, A. Bezryadin, S. de Vries, and C. Dekker, Nature **403** (2000) 635.

BL1A

Mo L_{III}-Edge XANES Study of MoO_3/H-MFI for GTL Catalysts

H. Aritani[1], S. Koyama[1], K. Otsuki[1], M. Fukushi[1], Y. Hoshino[1], S. Shinohara[1], A. Nakahira[2]
[1]*Department of Applied Chemistry, Saitama Institute of Technology, Okabe 369-0293, Japan*
[2]*Faculty of Engineering & Design, Kyoto Institute of Technology, Kyoto 606-8585, Japan*

MoO_3-modified H-MFI zeolite (MoO_3/H-MFI) is a typical catalyst for so-called GTL (Gas-To-Liquid) one, which process needs to produce aromatics from natural gas. Because methane is a dominant compound in natural gas, direct conversion from methane to benzene is a catalytically desired process. For MoO_3/H-MFI catalyst system, Mo species are reduced during the reaction at high temperature (at around 973 K), and Mo-carbide species are formed mainly as an active species for methane activation. Then dehydrogenated methane is formed as carbene-like species on reduced Mo species, and followed by production of benzene onto H-MFI. For the catalytic process described above, redox behavior of Mo ions is an important role for catalytic activity for dehydroaromatization of methane. In particular, formed Mo species after the reaction needs to analyze for evaluation of catalytically active sites. Thus we characterized the active Mo spices on H-MFI supports with various SiO_2/Al_2O_3 ratios by means of Mo L_{III}-edge XANES. In this report, local structure of supported Mo ions and their redox changes after dehydroaromatization of methane at 973 K for 3 h.

All the catalyst samples were prepared by impregnation of each silica-alumina support with AHM ($(NH_4)_6Mo_7O_{24}$•$4H_2O$) solution, and followed by drying and calcination at 773 K for 3 h. Amount of MoO_3-loading is 7.5wt% in all the samples. H-MFI supports were obtained by hydrothermal synthesis (at 343 K) from sodium silicate and aluminum chloride with TPABr template, and followed by filtration, H^+-ion exchanging with NH_4OH solution, and calcination at 773 K. Mo L_{III}-edge XANES spectra were collected in BL1A beamline of UVSOR-IMS in total-electron yield (TEY) mode. XANES spectra of reference Mo compounds were shown in the previous report.

Fig. 1 shows XANES spectra of MoO_3/H-MFI with various Si/Al_2 ratios before/after methane dehydroaromatization. Before reaction, Mo species on H-MFI are due to Mo^{6+} in all the ratios. It is likely that components of $Mo^{6+}O_6$ octahedra is larger than that of $Mo^{6+}O_4$ tetrahedra in low Si/Al_2 ratio. After the reaction of methane dehydroaromatization, edge energy of XANES spectra in all samples becomes low, indicating reduction of Mo ions. In case of H-MFI with Si/Al_2 = 90, the spectrum is almost as same as that of Mo_2C, while Mo_2C can not be detected by XRD. It possesses the formation of well-dispersed Mo-carbide species on H-MFI as highly reduced ones. On the other hand, the spectrum in Si/Al_2 = 40 shows Mo_2C and another components. The spectrum in Si/Al_2 = 1880 suggests formation of slightly reduced Mo sites partly. These results exhibit the highly reduction proceeds on H-MFI in Si/Al_2 = 90. These features can also be seen after ethene dehydroaromatization at 973 K. In fact, maximum benzene yield was obtained for MoO_3/H-MFI in Si/Al_2 = 90. It is concluded that formation of well-dispersed carbide species relates to the catalytic activity for GTL.

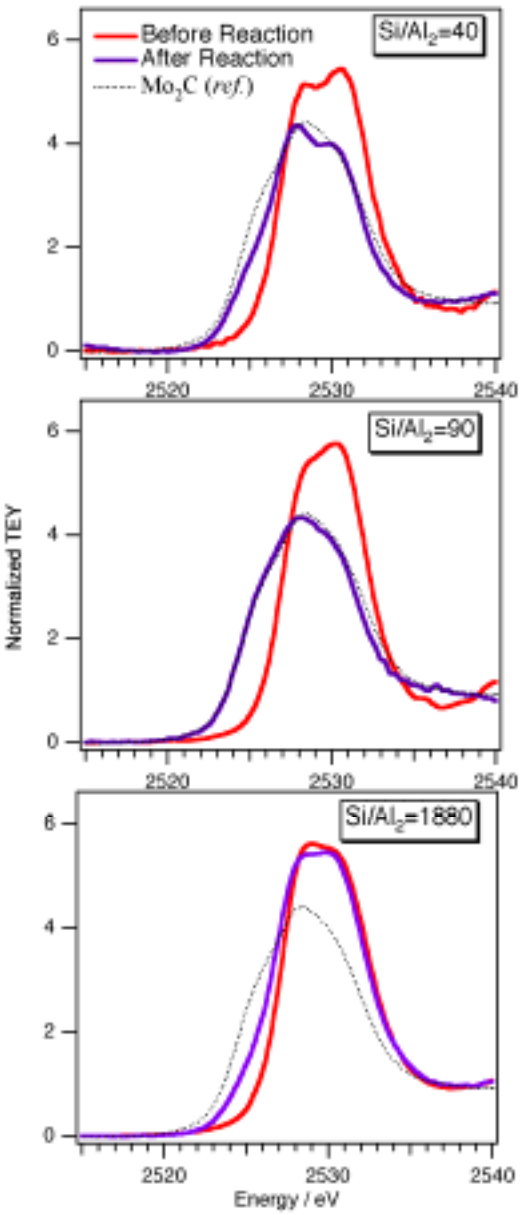

Fig. 1 Mo L_{III}-edge XANES spectra of MoO_3/H-MFI with various Si/Al_2 ratios before/after methane dehydroaromatization at 973 K.

BL1A

X-Ray Absorption Near-Edge Fine Structure Study of AlInN Semiconductors

Q. X. Guo[1], J. Ding[2], Y. Mitsuishi[1], T. Tanaka[1], M. Nishio[1], H. Ogawa[1]
[1]*Department of Electrical and Electronic Engineering, Saga University, Saga 840-8502, Japan*
[2]*Venture Business Laboratory, Saga University, Saga 840-8502, Japan*

With a wide variable bandgap range, AlInN has great potential for applications in light-emitting diodes and laser diodes. This is particularly true, because in their natural crystal structures both AlN and InN have direct bandgaps. Moreover, $Al_{0.83}In_{0.17}N$ can be used as a cladding layer with no strain on a GaN-based laser diode structure, leading to a reduction of defects because it is lattice-matched to GaN. In order to fulfill AlInN applications in commercially optical and electronic devices, many fundamental properties of this material should be clarified. X-ray absorption near-edge fine structure (XANES) refers to the region of the x-ray absorption spectroscopy spectrum dominated by strong photoelectron scattering that extends about 40 eV above an absorption edge, is a powerful tool to analyze electronic structures of materials, because spectral fine structure of XANES spectrum is very sensitive to a change in chemical environment. In this article, we report a characterization of AlInN using x-ray absorption measurements at the Al- *K* edges.

The AlInN thin films were prepared on (0001) sapphire substrates by reactive radio-frequency magnetron sputtering in an ambient of argon and nitrogen. The sputtering chamber was evacuated to a pressure of 10^{-7} Torr using a turbomolecular pump before introducing the sputtering gas. The sapphire substrates were chemically cleaned, degreased in organic solvents, etched in an acid solution, and then rinsed in deionized water. During the growth, the substrate temperature, total gas flow rate, and pressure were maintained at 100°C, 3 sccm, and 10 mTorr, respectively. The indium plate and the aluminum plate were separately mounted onto the targets and the sputtered area was varied in order to obtain AlInN films with the desired composition.

The XANES experiments were carried out at beam line BL1A of UVSOR facility in the Institute for Molecular Science, Japan. The XANES spectra were collected by recording the total yield of secondary electrons at room temperature. The photon flux was obtained simultaneously by measuring the current of an Au mesh located near the exit slit of the monochromator and used for normalization of the XANES spectra. Figure 1 shows the Al *K*-edge XANES spectra of $Al_xIn_{1-x}N$ films at various Al compositions x. As shown in Fig.1, all the characteristics of XANES spectra, including the position and the slope of the absorption edge as well as the energy positions and the intensities of the resonances, depend strongly on the composition. The main peak labeled B is clearly observed in all samples which include Al content. Its intensity increases with increasing Al content, although no linear relationship is observed because the intensity depends on both the Al content and the sample thickness and size. Therefore, we believe that the XANES spectrum can be a fingerprint of the composition of the nitride semiconductors since it is affected both by the central-absorbing atom and its neighboring atoms. Here, we note that the peak positions (A, B, and C) in Fig. 1 shift to lower energy with decreasing Al content.

Next, the XANES spectra of Al *K*-edge in wurzite AlInN was computed on the basis of the self-consistent-field real-space multiple-scattering (RSMS) theory calculations using the FEFF8 code. We find that the experimental and theoretical XANES spectra are in satisfactory agreement. Both the experimental curve shape and peak positions are reasonably reproduced in the theoretical spectra although there are some shifts in peak positions as well as differences in intensity. This discrepancy may be due to errors in the theory; for example, errors in the self-energy or the neglect of nonspherical corrections to the potential.

In conclusion, we have carried out the XANES measurements of AlInN at Al *K*-edge and the self-consistent-field real-space multiple-scattering theory calculations using FEFF8 code. It was demonstrated that the Al K-edge XANES spectra of AlInN are the fingerprints of their composition. The theoretical results could give a reasonable reproduction of the experimental spectral structures. This type of combined use of the experimental XANES and the RSMS calculations must be a powerful tool for systematic and qualitative analysis of the structural and electronic structures of nitride semiconductors.

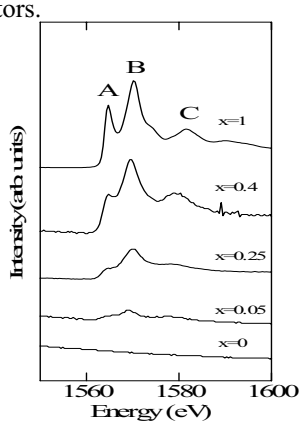

Fig. 1 Experimental Al *K*-edge XANES spectra for $Al_xIn_{1-x}N$.

BL1A&8B1

Study on the Surface Structure of Cathode Electrode for Li-Ion Battery Cells with High Power-Type

H. Kobayashi[1], Y. Arachi[2], S. Emura[3]

[1]*Research Institute for Ubiquitous Energy Devices, AIST, Ikeda, Osaka, 563-8577 Japan*

[2]*Unit of Chemistry, Faculty of Engineering, Kansai University, Suita, Osaka, 564-8680 Japan*

[3]*ISIR, Osaka University, Ibaraki, Osaka, 567-0047 Japan*

Lithium ion battery has attracted the interest on the application for fuel cell vehicle (FCV) because of the promising high-power sources. On the other hand, the battery for FCV requires the long period life over 15 years. Therefore, the development of the estimation method of the pulse cycle and calendar life has been strongly needed and several mechanisms have been proposed to explain the deterioration in battery performance. Although the deterioration in battery performance has instinct problem on the electrodes, the mechanism of deterioration on the electrodes is still unclear. Detailed information on the change in the both cathode and anode electrodes is very important in order to determine the origin of battery performance of electrochemical performance of battery cell. In this study, the XANES spectra about the cathode electrode after pulse cycle tests were collected by the total electron yield (TEY) method and the relationships between the changes in the surfaces and their electrochemical properties were studied.

Experimental

We used the cylindrical battery cells of c.a. 400 mAh for this study. $LiNi_{0.8}Co_{0.2}O_2$-based material and hard carbon were used for positive and negative electrode, respectively. Each cell was characterized using standard battery test procedure given in the partnership for a new generation of vehicles (PNGV) Battery Test Manual. We checked the changes in the cell capacity and DC resistance at every several cycles. The SOC0% and SOC100% cathode electrode obtained from the battery after PNGV tests were washed with DMC and then Ni/Co *L*-edges and O *K*-edge were measured by the TEY method on BL1A or BL8B1 at UVSOR, respectively.

Results

The results after pulse cycle tests are summarized in Table 1. The decrease in capacity and increase in DC resistance were observed with increasing temperature. These results indicated that battery performance deteriorated when battery cells were used at high temperature. ICP and XRD results indicated that the valence state of Ni and Co increased to higher valence state for SOC0% samples and the valence state of Ni and Co decreased to lower valence state for SOC100% samples after the pulse cycle tests in this system, and showed that no degradation of crystallinity and appearance of impurity phases were observed for cathode material. On the other hand, both Ni and Co *L*-edges XANES results of SOC0% and 100% samples showed the shifts of L_{III} and L_{II} peaks to higher energy above 40°C, indicating the increase in the valence state of Ni and Co on the surface. Figure 1 shows Ni *L*-edge XANES spectra for the SOC100% cathode materials. In addition, the O *K*-edges XANES spectra of SOC100% sample after test at 60ºC showed the additional peak similar to NiO together with pre-edge peak originated from $LiNi_{0.8}Co_{0.2}O_2$-based phase, indicating the existence of cubic phase on the surface. These XANES results indicated that the surface structure became to be different from bulk one after pulse cycle tests. The TEY method using soft X-ray gave us useful information to understand the origin of battery performance of battery performance.

Table 1 Results of pulse cycle test.

	I^P_{max}	DOD	Cycles	Relative Capacity	Relative DC resistance
20ºC	10C	3%	50000	0.960	1.08
40ºC	10C	3%	50000	0.946	1.11
40ºC	20C	3%	50000	0.951	1.13
40ºC	10C	30%	3000	0.932	1.25
60ºC	10C	3%	50000	0.907	1.28

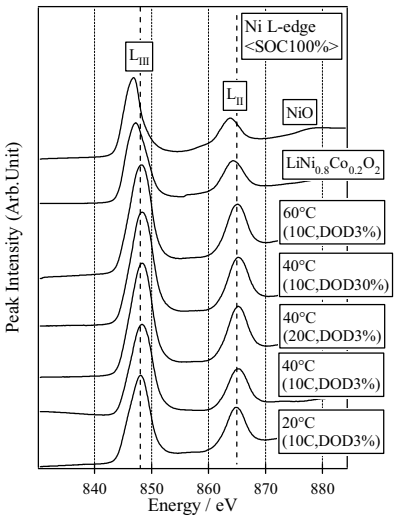

Fig. 1 Ni *L*-edge XANES spectra for the cathode materials. NiO and $LiNi_{0.8}Co_{0.2}O_2$ are given as reference.

Acknowledgement

This work was supported by Ministry of Economy, Trade and Industry (METI) and New Energy and Industrial Technology Development Organization (NEDO).

BL1A&8B1

Crystal and Electronic Structures of the $LiNi_{0.45}Mn_{0.45}Al_{0.10}O_2$

H. Kobayashi[1], I. Teshima[2]

[1]*Research Institute for Ubiquitous Energy Devices, AIST, Ikeda, Osaka, 563-8577 Japan*

[2]*Department of Molecular Science and Technology, Faculty of Engineering, Doshisha University, Kyotanabe, Kyoto, 610-0321 Japan*

$LiNi_{1/2}Mn_{1/2}O_2$-based materials are one of the promising cathode materials of lithium secondary battery because of their large capacity and high thermal stability. Especially, $LiNi_{1/3}Mn_{1/3}Co_{1/3}O_2$ displays a reversible capacity of 170 mAh/g in the voltage range 2.5 to 4.5 V and keep the layered structure over 280 C° [1]. A lot of papers have reported on electrochemical performance of the $Li_{1-y}Ni_{1/2}Mn_{1/2}O_2$-based materials until now. We have studied these materials from the perspective of structure and found the characteristic structural change during Li de-intercalation for $LiNi_{1/2}Mn_{1/2}O_2$ [2]. On the other hand, the relationship between the crystal and electronic structures are still ambiguous in these systems. Detailed information on the electronic structures is very important in order to improve the electrochemical properties of these materials and, therefore, the crystal and electronic structures of $LiNi_{0.45}Mn_{0.45}Al_{0.10}O_2$ were investigated in this study.

Experimental

$LiNi_{0.45}Mn_{0.45}Al_{0.10}O_2$ was synthesized in air at 1273 K for 24 h using appropriate molar ratios of $LiOH{\cdot}H_2O$, $Mn(CH_3COO)_2{\cdot}6H_2O$, $Ni(CH_3COO)_2{\cdot}6H_2O$, and $AlNO_3$. The de-lithiated samples were prepared electrochemically using coin-type cells with Li/1M $LiPF_6$ in EC:DEC(1:1)/samples. Crystal and electronic structures were investigated by synchrotron XRD (BL02B2 at SPring-8), XAFS (BL7C at PF), and the total electron yield (BL1A/BL8B1 at UVSOR) measurements. The crystal structure was determined using the computer program RIETAN2000.

Results

$LiNi_{0.45}Mn_{0.45}Al_{0.10}O_2$ was single-phase and adopted the α-$NaFeO_2$ structure. The Ni and Co *K*-edge XANES spectra showed that $LiNi_{0.45}Mn_{0.45}Al_{0.10}O_2$ can be represented as $Li(Ni^{2+}{}_{0.45}Mn^{4+}{}_{0.45}Al^{3+}{}_{0.10})O_2$. Structural analysis using synchrotron XRD data demonstrated that the lattice parameters of $LiNi_{0.45}Mn_{0.45}Al_{0.10}O_2$ are a = 2.881 Å and c = 14.31 Å and that the chemical composition can be expressed referring to the Wyckoff positions 3*a* and 3*b* with the space group *R3m* as $[Li_{0.92}Ni_{0.08}]_{3a}$ $[Li_{0.08}Mn_{0.45}Ni_{0.37}Al_{0.10}]_{3b}O_2$. The fraction of Ni on the 3*a* site is almost equal to be those observed for $LiNi_{0.5}Mn_{0.5}O_2$ and $LiNi_{0.5}Mn_{0.4}Ti_{0.1}O_2$ [3]. $Li_{1-y}Ni_{0.45}Mn_{0.45}Al_{0.10}O_2$ corresponded to the composition for showing a charge capacity of 170 mAh/g. Figure 1 shows the Ni *L*-edge and O *K*-edge XANES spectra in $Li_{1-y}Ni_{0.45}Mn_{0.45}Al_{0.10}O_2$. The Ni *L*-edge XANES results showed that divalent nickel metal is oxidized to tetravalent through trivalent after charging, while the O *K*-edge showed no change over the whole composition range. These results clarified that the Li de-intercalation/ intercalation from $LiNi_{0.45}Mn_{0.45}Al_{0.10}O_2$ proceeded mainly by the valence state change of Ni without the contribution of oxygen over the whole composition range.

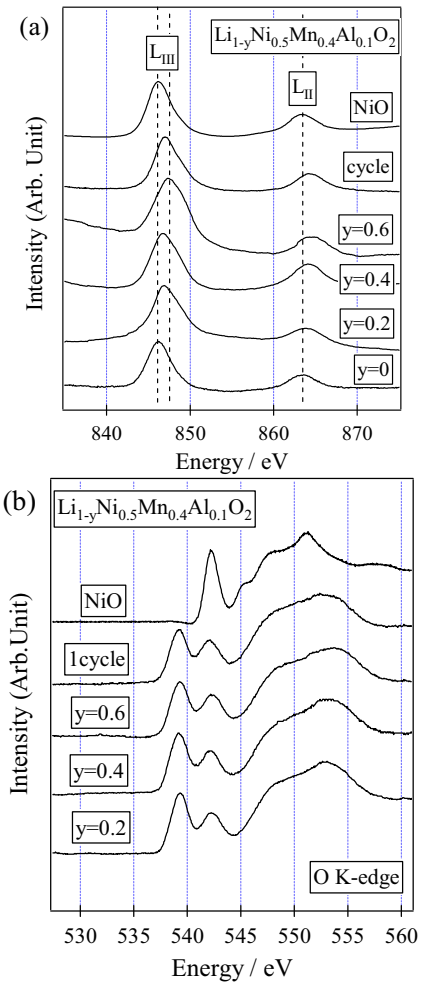

Fig. 1 Ni *L*-edge (a) and O *K*-edge (b) XANES spectra in $Li_{1-y}Ni_{0.45}Mn_{0.45}Al_{0.10}O_2$.

[1] N. Yabuuchi and T. Ohzuku, J. Power Sources. **119-121** (2003) 171-174.

[2] H. Kobayashi, Y. Arachi, K. Tatsumi, and H. Kageyama, J. Mater. Chem. **14** (2004) 40-42.

[3] H. Kobayashi, Y. Arachi, H. Kageyama, H. Sakaebe, K. Tatsumi, D. Mori, R. Kanno, and T. Kamiyama, Solid State Ionics. **175** (2004) 221-224.

BL1A

Investigation of Local Structure for Low Crystalline Calcium Phosphate Prepared by Anodic Oxidation of Ti Metal

A. Nakahira[1], H. Aritani[2], K. Konishi[1], S. Nishida[1], K. Kubo[1], S. Takaezoe[1], M. Ohta[1]

[1]*Faculty of Engineering & Design, Kyoto Institute of Technology, Matsugasaki, Sakyo, Kyoto 606-8585, Japan*

[2]*Faculty of Engineering, Saitama Institute of Technology, Okabe, Saitama 369-0293, Japan*

Introduction

In biomaterials, hydroxyapatite and calcium phosphates are expected to be used as an implant material. Since especially, calcium phosphate and hydroxyapatite with low crystallinity, not high crystallinity, are active for bone formation, the developments of low crystalline calcium phosphate and hydroxyapatite are desired. On the other hand, Ti metal is also one of the useful implant materials. However, Ti metal has no bioactivity for bone formation in body. Therefore, the calcium phosphate coating on Ti metal is important process for the achievement of the high bioactivity for Ti implants. In general, coatings of calcium phosphate are carried out by sol-gel coating and arc plasma methods. Recently, many studies on anodic oxidation of Ti metal are titanium oxide films prepared by are reported for novel developments of titanium oxides and other oxides coating on Ti metal. In addition, this anodic oxidation method is considered to be useful to prepare the calcium phosphate materials on Ti. In special, doping some anions into oxide is easy to perform by anodic oxidation methods.

In this study, the low crystalline calcium phosphate samples were synthesized by an anodic oxidation of Ti metal using the mixture of calcium salts and H_3PO_4 solution at room temperature. Because in medical application, this low crystalline calcium phosphates are more effective for the osteoconduction, compared to high crystalline calcium phosphate, the information of low crystalline calcium phosphates are considered to be useful for developing the high performance implant materials. The purpose is to clarify the local structure of P ion in low crystalline calcium phosphate. The investigation of local structure for this low crystalline calcium phosphate prepared by the anodic oxidation method was carried out at BL1A in UVSOR.

Experiment

Ti metal (10 mm × 10 mm × 0.4 mm) was used as an anode and carbon black (φ5 mm × 10 mm, Toyo carbon) was used as a cathode. The distance between electrodes was about 3 cm. Ti substrate was polished using abrasive paper. Finally it was washed with dionized water and dried in atmosphere before it was used as an electrode. After polishing, the Ti substrate was soaked in solution mixed with glycerophosphoric acid calcium salt (GP) and H_2O. Anodic oxidation performed under 50 V, 150 V, 250 V, and 350 V supplied direct current power.

Results and Discussion

The samples obtained by the anodic oxidation in this experiment were identified to be a calcium phosphate with low crystallinity by the results of powder X-ray diffraction analysis. P-*K* local structure for this low crystalline calcium phosphate prepared by the anodic oxidation method was examined at BL1A in UVSOR. The XANES spectra of low crystalline calcium phosphates obtained by anodic oxidation in solution mixed with GP and H_2O are shown in Figure 1 (shown by GP-Anodic Oxidation in figure). All spectra of low crystalline calcium phosphates synthesized by anodic oxidation were similar, although the low crystalline calcium phosphates obtained by anodic oxidation at higher voltage of 50 V and 350 V possess P^{5+}. From these results of XANES spectra at P-*K* edge, P local structures for low crystalline calcium phosphates synthesized by anodic oxidation method of Ti was similar to those of $Ca_2P_2O_7$., not hydroxyapatite (HAP). These results will lead to the development of the high performance implant materials.

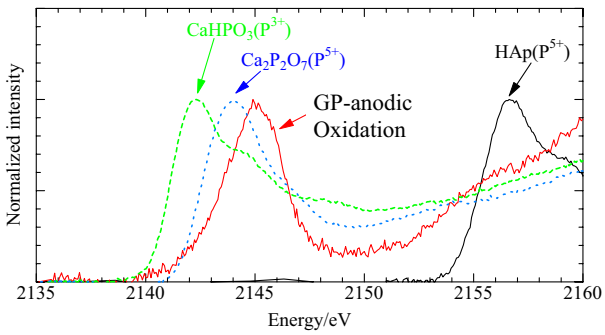

Fig. 1 XANES of P-*K* edge of low crystalline calcium phosphates. GP-ampdic oxidation was the sample synthesized by an anodic oxidation processing. HAP shows hydroxyapatite. $CaHPO_3$ and $Ca_2P_2O_7$ are reference materials.

BL1A

Investigation of Local Structure of P-*K* Edge for Titania Prepared by Anodic Oxidation of Ti Metal

A. Nakahira[1], H. Aritani[2], K. Konishi[1], S. Nishida[1], K. Kubo[1], S. Takaezoe[1], M. Ohta[1]

[1]*Faculty of Engineering & Design, Kyoto Institute of Technology, Matsugasaki, Sakyo, Kyoto 606-8585, Japan*

[2]*Faculty of Engineering, Saitama Institute of Technology, Okabe, Saitama 369-0293, Japan*

Titaniumu oxide (titania) is one of useful materials for photocatalyst, although titania is classified into anatase-type, rutile-type, and brookite-type. Usually, various synthesis methods, such as sol-gel, sputtering, chemical processings, and so on, have been reported by many researchers for the synthesis of titania. Although, in general, the coatings of titania on Ti substrate are carried out by sol-gel coating and arc plasma methods, these coatings have such problems that the strength between titania and Ti is weak and sometimes the delamination is generated between titania and Ti. On the other hand, anodic oxidation method of Ti metal is a unique method for preparation of strong titania coating on Ti metal. Furthermore, In addition, this anodic oxidation method is considered to be significantly useful to prepare the high performance titania coating with doping some anions. Namely, it is expected that such doping into titania is easy to perform by this anodic oxidation methods. So, this anodic oxidation will be applicable for the modification of titania by successful doping of various ions into titania on titanium metal for photocatalyst.

In this study, the various synthesis of titania doped of P ion was attempted by an anodic oxidation of Ti metal using the mixture of H_3PO_4 solution at various temperatures ranging room temperature and 343 K. The investigation of local structure, in main XANES, for this P-doped titania prepared by the anodic oxidation method in this study was carried out at BL1A in UVSOR.

Experiment

Ti metal (10 mm × 10 mm × 0.4 mm, Nilaco. Co. ltd) was used as an anode and carbon black (φ5 mm × 10 mm, Toyo carbon) was used as a cathode. Ti substrate was polished using abrasive paper, washed with deionized water and finally dried in atmosphere before it was used as an electrode. The distance between electrodes on anodic oxidation processing was kept to be approximately 3 cm. Ti substrate was soaked in solution mixed with glycerophosphoric acid sodium salt (Na-GP) and aqueous H_3PO_4 at room temperature. Other samples were synthesized in the mixture of glycerophosphoric acid calcium salt (Ca-GP) and aqueous H_3PO_4 solution at room temperature. For comparison, Ti substrate was soaked only in aqueous H_3PO_4 solution. Anodic oxidation processing in this study was performed under a voltage of 350 V supplied with direct current power (TP0650-01, Takasago Seisakusho, Co. Ltd, Japan).

Results and Discussion

The samples obtained by anodic oxidation processing at a voltage of 350 V were identified to be anatase with low crystallinity by powder X-ray diffraction analysis. P-*K* local structure for these low crystalline titania samples prepared by the anodic oxidation method was examined at BL1A in UVSOR. Figure 1 shows the results of XANES of P-*K* of some titania samples prepared by anodic oxidation method and also some reference materials. The XANES spectra of titania obtained by anodic oxidation were similar to one of $Ti_3(PO_4)_4$, although the position of its peak was not agreement with ones of other references. From these results of XANES spectra at P-*K* edge, P local structures of titania with low crystallinity prepared by onodic oxidation method was almost similar to one of $Ti_3(PO_4)_4$.

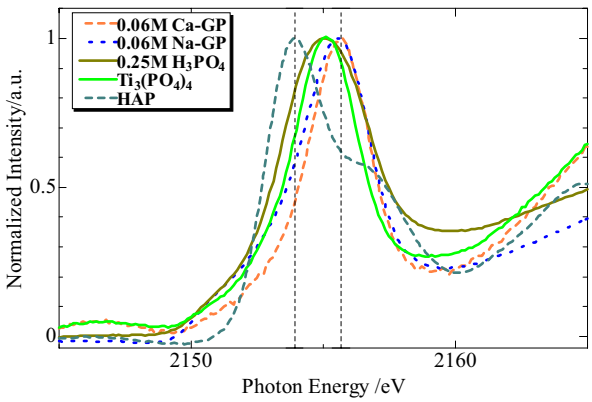

Fig. 1 XANES of P-*K* of some titania samples prepared by anodic oxidation method. Ca-GP samples were synthesized in the mixture of glycerophosphoric acid calcium salt (Ca-GP) and aqueous H_3PO_4 solution at room temperature. Na-GP samples were synthesized in the mixture of glycerophosphoric acid sodium salt (Na-GP) and aqueous H_3PO_4 solution at room temperature.

BL1A

Characterization of Mixed Valence Complexes of Platinum by an XAFS Method

H. Yamashige[1], K. Kuroiwa[2], T. Kurisaki[1], H. Wakita[1,3]

[1]*Department of Chemistry, Faculty of Science, Fukuoka University, Nanakuma, Jonan-ku, Fukuoka 814-0180, Japan*

[2]*Department of Chemistry and Biochemistry, Graduate School of Engineering, Kyushu University, Higashi-ku, Fukuoka 812-8581, Japan*

[3]*Advanced Materials Institute, Fukuoka University, Nanakuma, Jonan-ku, Fukuoka 814-0180, Japan*

There has recently been much interest in the one-dimensional (1D) halogen-bridge metal complexes [1], because of their unique physical properties in the mixed-valence state or, equivalently, the commensurate charge density wave (CDW) state.

In this work, we applied X-ray absorption fine structure (XAFS) spectroscopy to structure analysis of the 1D chloro-bridged Pt complexes: $[Pt^{II}(en)_2][Pt^{IV}(en)_2Cl_2]X_4$ (X= ClO_4, Glu, Asp). The X-ray absorption spectra were measured at BL1A of the UVSOR in the Institute of Molecular Science, Okazaki [2]. The energy of the UVSOR storage ring was 750 MeV and the stored current was 110-230 mA. Cl *K*-edge absorption spectra were recorded in the region of 2533-3733 eV by use of two Ge(111) crystals. The absorption was monitored by the total electron yield using a photomultiplier. The Cl *K* XANES spectra for three Pt complexes are shown in Fig. 1. A pre-edge peak and a main peak are observed in these spectra.

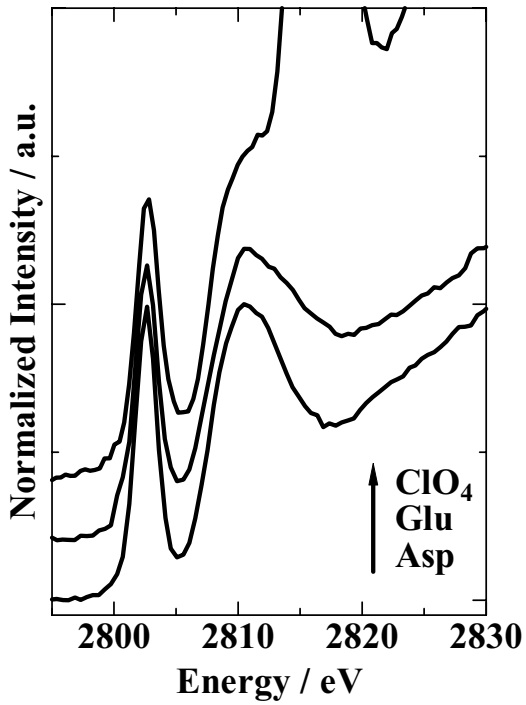

Fig. 1 Observed Cl *K*-edge XANES spectra of $[Pt^{II}(en)_2][Pt^{IV}(en)_2Cl_2]X_4$,(X= ClO4, Glu, Asp).

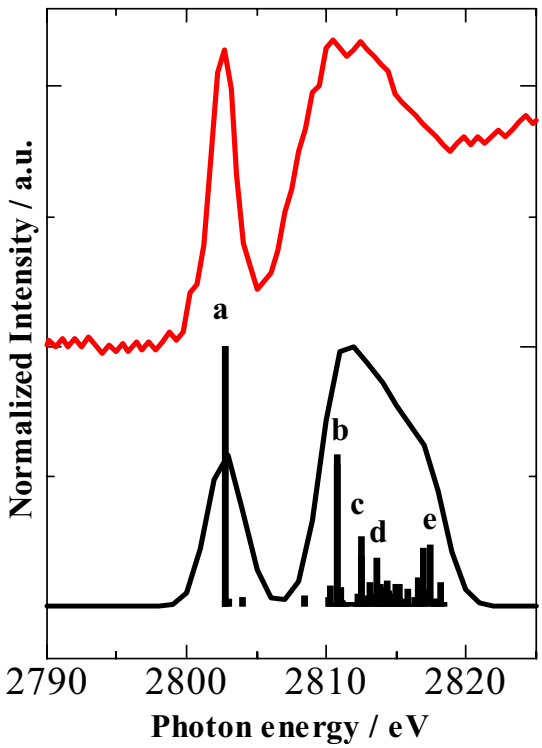

Fig. 2 Observed and calculated Cl *K*-edge XANES spectra of $[Pt^{II}(en)_2][Pt^{IV}(en)_2Cl_2](Glu)_4$.

Observed and calculated Cl *K* XANES spectra for the $[Pt^{II}(en)_2][Pt^{IV}(en)_2Cl_2](Glu)_4$ complex are shown in Fig. 2.The two peaks are estimated to the electron transition (pre-edge peak: Cl 1*s* to Pt 5*d*, main peak: Cl 1*s* to mixed orbital). As a result of many other calculated data, the energy gap of two peaks is related to the distance between Pt and Cl atoms.

[1] P. Day, in H. J. Keller (eds.), *Low Dimensional Cooperative Phenomena* (Plenum, New York, 1974) 191.

[2] S. Murata, T. Matsukawa, S. Naoè, T. Horigome, O. Matsuodo, and M. Watatabe, Rev. Sci. Instrum. **63** (1992) 1309.

BL5U

Three-Dimensional Band Dispersion of $CeTe_2$

T. Ito[1,2], H. J. Im[2], S. Kimura[1,2], Y. S. Kwon[3]

[1]*UVSOR Facility, Institute for Molecular Science, Okazaki 444-8585, Japan*

[2]*School of Physical Science, The Graduate University for Advanced Studies, Okazaki 444-8585, Japan*

[3]*BK21 Physics Research Division and Institute of Basic Science, Sungkyunkwan University, Suwon 440-746, Korea*

Low-dimensional compounds have attracted much attention because of their anomalous electronic/magnetic properties, especially the coexistence of the charge density wave (CDW) formation and the antiferro-magnetism. Since their anomalous properties have been attributed to the low dimensionality, in turn, the three–dimensionality at the electronic structure is important to understand the essential nature of the anomalous properties.

Angle-resolved photoemission spectroscopy (ARPES) is one of powerful methods to directly determine the electronic band structure as well as the Fermi surface topology. However, there are few examples of the ARPES determination of the three-dimensional electronic structure by controlling the excitation energy and the detecting angle. To elucidate the three dimensionality at the electronic structure of low-dimensional compounds, we have performed the photon-energy dependent ARPES on the quasi-two dimensional $CeTe_2$, which crystallizes in the layered structure formed by the planar Te(1) sheet sandwiched by the corrugated CeTe(2) double layers [1].

Figure 1 shows the photon-energy dependence of the ARPES spectra of $CeTe_2$ at normal emission ($k_{//}$ = 0 $Å^{-1}$), obtained at UVSOR-II BL5U with using synchrotron radiation source. Since the control of the photon-energy at $k_{//}$ = 0 $Å^{-1}$ directly corresponds to the trace of the electronic structure along ΓZ axis, we have mapped out the dispersive feature of the ARPES peaks as a function of photon energy and binding energy. Here, we use the dispersion relation

$$(h/2\pi)k_{\perp} = \sqrt{2mE_K\cos^2\theta + V}\ ,$$

where V is inner potential, E_K is kinetic energy at E_F and θ = 0°. At the left panel in Fig. 2, we show the experimental band structure along ΓZ line where V ~ 15 eV is expected from the symmetry of the dispersive features. In Figs. 1 and 2, we clearly find the two types of bands; one is almost non-dispersive bands at 0.5 and 1.0 eV binding energies, and the other is the bands with a large dispersion from 1.0 eV (1.8 eV) to 1.5 eV (< 1.7 eV) along ΓZ line. From the comparison with the band calculation of the reference compound $LaTe_2$ (right panel in Fig. 2), the former has been attributed to the Te 5*p* orbital at the Te(1) plane (green lines), while the latter to one at the CeTe(2) plane (blue lines). The observed highly-dispersive feature may suggest the possible three-dimensionality on the electronic structure of quasi-two dimensional $CeTe_2$.

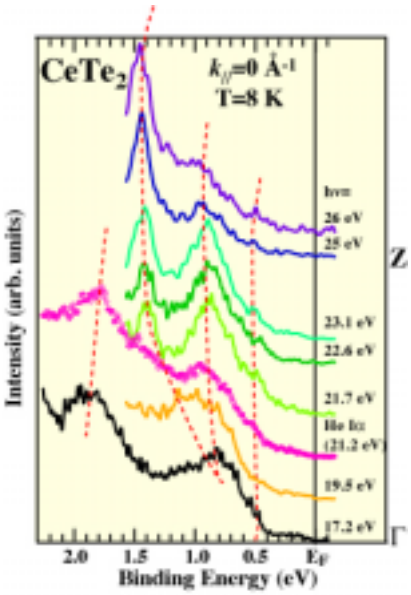

Fig. 1 Photon-energy dependence of ARPES spectra of $CeTe_2$. Note that the spectrum with hν = 21.2 eV is obtained by using the He Iα resonance line.

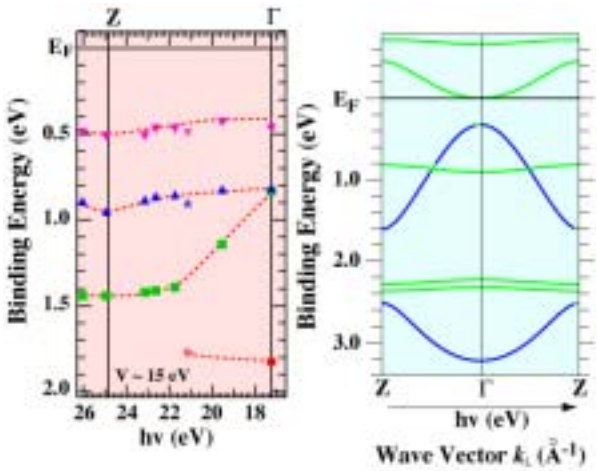

Fig. 2 (Left panel) Experimental band structure along ΓZ high-symmetry line of $CeTe_2$. Symbols and dashed lines are the ARPES peak positions and guide for eyes, respectively. (Right panel) LDA band calculation along ΓZ high-symmetry line of $LaTe_2$.

[1] M.H. Jung *et al.*, Phys. Rev. B **62** (2000) 11609.

BL5U

Ce 4*d* - 4*f* Resonant Photoemission Spectroscopy on $CeNi_{1-x}Co_xGe_2$

H. J. Im[1], T. Ito[1,2], B. K. Lee[3], S. Kimura[1,2], Y. S. Kwon[3]

[1]*School of Physical Science, The Graduate University for Advanced Studies, Okazaki 444-8585, Japan*

[2]*UVSOR Facility, Institute for Molecular Science, Okazaki 444-8585, Japan*

[3]*BK21 Physics Research Division and Institute of Basic Science, Sungkyunkwan University, Suwon 440-746, Korea*

$CeNi_{1-x}Co_xGe_2$ were newly found Ce-based ternary alloys, where the ground states continuously change from a local-moment magnetism (x = 0 – 0.2) to an intermediate valence (x = 0.4 – 1.0) regimes through a quantum-critical point (QCP) (x = 0.3) by the hybridization between the Ce 4*f* and Ni/Co 3*d* states with the similar lattice constants in this series [1]. To elucidate the systematic change of the electronic (magnetic) structure as a function of the *d* - *f* hybridization strength through QCP, we have performed Ce 4*d* - 4*f* resonant photoemission (RPE) spectroscopy on $CeNi_{1-x}Co_xGe_2$ with varying the Co - substitution from x = 0 to x = 1.0.

Polycrystalline $CeNi_{1-x}Co_xGe_2$ were grown by the arc-melting and annealed at 900°C for 3 weeks in an evacuated quartz tube. The Ce 4*d* – 4*f* RPE measurements were carried out at UVSOR-II BL5U with the energy resolution of about 150 meV at hν = 122 and 115 eV which correspond to Ce 4*d* – 4*f* on- and off- resonance energies, respectirvely. The clean surfaces were prepared by fracturing the polycrystalline samples *in situ* under vacuum of 2 x 10^{-8} Pa. The Fermi level of the sample was referred to a gold film evaporated onto the sample substrate.

Figure 1 shows the Co-substitution dependence of the Ce 4*d* – 4*f* on- (upper panel) and off– (lower panel) RPE spectra measured at *T* = 5 K. While the off– RPE spectra are formed by the Ni/Co 3*d* main peaks around 1.8/0.6 eV, the on– RPE spectra show additional structures around 2 and 0.3 eV where the strong Ce 4*f* character has been expected by the single-impurity Anderson model (SIAM) [2]. With increasing Co– substitution, *d* - states shift from 1.8 to 0.6 eV in the off– RPES spectra and the spectral weight at E_F seems to be enhanced in consistent with the corresponding LDA band calculation. On the other hand, the spectral weight of Ce 4*f* structures transfers from 2.2 eV to 0.3 eV. From the comparison with the SIAM calculation on the various kind of Ce–based heavy fermion compounds [2], we have assigned that the former Ce 4*f* structure comes from the Ce $4f^0$ final states with a localized Ce 4*f* character, while the latter from the Ce $4f^1$ final states with a itinerant (or strongly hybridized) Ce 4*f* electrons. Thus, the systematic changes of the *d* – bands and the Ce 4*f* states may be attributed to the increased *d*– *f* hybridization strength from the localized $CeNiGe_2$ to the itinerant $CeCoGe_2$.

Finally, we can briefly comment on the change of the electronic structure around QCP. It has been expected by the thermodynamic experiments that the Ce 4*f* electronic structures show anomaly at QCP [1]. On the other hand, the Ce 4*f* electronic structures around 2.2 and 0.3 eV in Fig. 1 show no anomalous change between x = 0.2 and x = 0.4. We can say that the observed contradiction strongly suggests the continuous change of the Ce 4*f* electronic structures from localized to itinerant regime, at least, in the valence band region. To elucidate the relation between the anomalous properties at QCP and the systematic change of the Ce 4*f* electronic structures through QCP, further studies (detailed analysis based on SIAM, temperature dependent RPE experiments, etc) are intended.

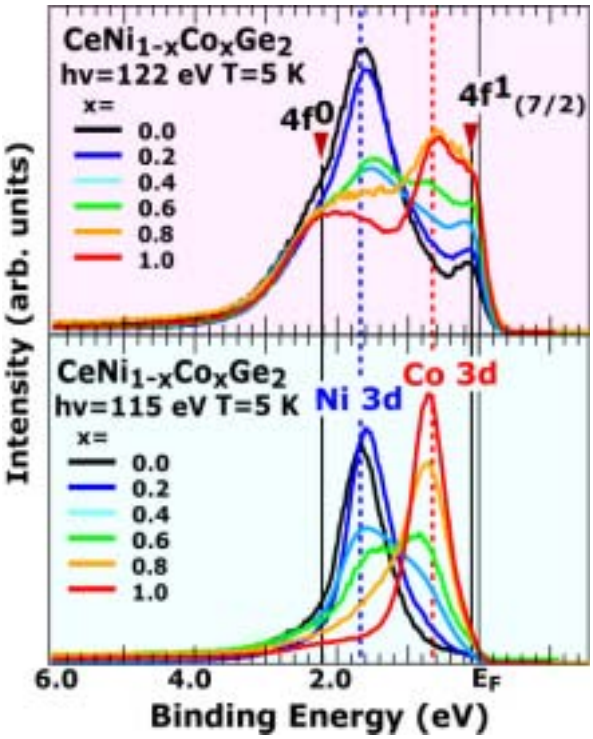

Fig. 1 Co-substitution dependence of the Ce 4*d* - 4*f* on - (Upper panel) and off – RPE spectra (lower panel), obtained with using hν = 122 eV and 115 eV photons at *T* = 5 K, respectively.

[1] B. K. Lee *et al.*, Phys. Rev. B (2005) in press.
[2] For example, D. Malterre *et al.*, Adv. Phys. **35** (1986) 275.

BL5U

Electronic Structure of Zr-TM-Al (TM = Ni, Cu) Bulk Metallic Glasses

K. Soda[1], T. Suzuki[1], H. Miyazaki[1], M. Inukai[1], M. Kato[1], S. Yagi[1], T. Takeuchi[2], U. Mizutani[1], T. Taketomi[3], M. Hasegawa[3], T. Ito[4], S. Kimura[4]

[1]*Graduate School of Engineering, Nagoya University, Furocho, Chikusa-ku, Nagoya 464-8603, Japan*

[2]*Ecotopia Science Institute, Nagoya University, Furocho, Chikusa-ku, Nagoya 464-8603, Japan*

[3]*Institute for Materials Research, Tohoku University, Katahira, Aoba-ku, Sendai 980-8577, Japan*

[4]*UVSOR, Institute for Molecular Science, Myodaijicho, Okazaki 444-8585, Japan*

Introduction

Bulk metallic glasses are new materials having useful engineering properties such as high mechanical strength, good ductility, and high corrosion resistance. In order to understand the origins of their large glass formation ability and unique properties from the microscopic point of view, we have studied the electronic structure of bulk metallic glasses Zr-TM-Al (TM = Ni, Cu) by use of photoelectron spectroscopy.

Experimental

Photoelectron spectra were recorded under an ultrahigh vacuum of 2 x 10^{-8} Pa at low temperatures with a high-resolution energy analyzer at BL5U. Total energy resolution and the origin of the binding energy E_B, *i.e.* the Fermi level E_F, were determined by the Fermi edge of an evaporated Au film.

Specimens were bulk metallic glasses $Zr_{65}Ni_{25}Al_{10}$, $Zr_{50}Cu_{35}Al_{15}$, $Zr_{66.7}Cu_{25.8}Al_{7.5}$, and $Zr_{55}Al_{10}Cu_{30}Ni_5$ in a size of ϕ 2 mm x 3 mm and attached on a cupper plate by conductive glue. Their supercooled liquid regions $\Delta T_x = T_x - T_g$ (T_x: crystallization temperature, T_g: glass transition temperature), one of the parameters representing the stability of these metallic glasses, are 52.0 K, 61.8 K, 99.8 K and 87.9 K, respectively. Clean surfaces for the measurement were prepared by *in situ* scraping the specimen with a diamond file.

Results and Discussions

Figure 1 shows typical valence-band photoelectron spectra of the metallic glasses recorded at 30 K with the excitation photon energy $h\nu$ of 40 eV. They are normalized by the intensity integrated up to the binding energy E_B of 10 eV. Three features around E_B = 0.6 eV, 2.0 eV and 3.7 eV are ascribed to the Zr 4*d*, Ni 3*d* and Cu 3*d* states, respectively. It seems that the peak positions of the Zr 4*d*-derived bands, indicated by arrows in the figure, are located at the higher binding energy as the metallic glass is more stable. This may imply that the hybridization of Zr 4*d* states with the states of its neighboring atoms, or the chemical bonding around Zr, becomes strong with the stability.

Valence-band spectra near E_F recorded with $h\nu$ = 18 eV are shown in Fig. 2 for the metallic glasses and a reference Au. The detailed analysis shows that the intensity is reduced in comparison with Au below the binding energy indicated by arrows, which suggests that a pseudo-gap in the *sp* bands of these glasses may increase with the phase stability [1].

The present results show how the electronic states of the metallic glasses contribute to their large glass formation ability. Further systematic study is intended for Zr-Ni-Al and Zr-Cu-Al metallic glasses with different compositions.

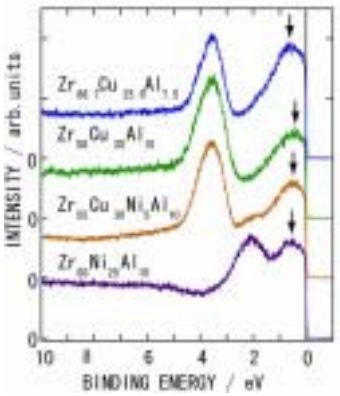

Fig. 1 Valence-band spectra of Zr-TM-Al (TM = Ni, Cu) recorded with $h\nu$ = 40 eV.

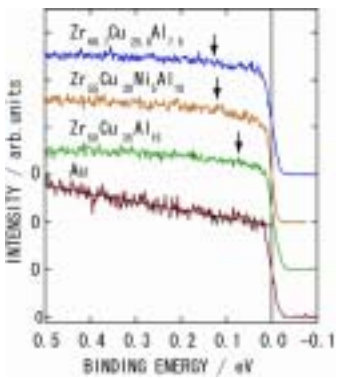

Fig. 2 Valence-band spectra near the Fermi level of Zr-TM-Al (TM = Ni, Cu) and Au recorded with $h\nu$ = 18 eV.

[1] K. Soda *et al.*, J. Electron Spectrosc. & Relat. Phenom., *in press*.

BL5U

Surfaced Photo-Voltage Effect on Cr/GaAs(100) Surface Studied by Combination of SR and Laser

K. Takahashi, Y. Nagata, S. Tokudomi, J. Azuma, M. Kamada
Synchrotron Light Application Center, Saga University, Saga 840-8502 Japan

Electronic non-equilibrium in the surface layer of photo-excited metal/semiconductor interfaces has been attracting much interest from the basic scientific point of view and also from the practical applications for photo-electronic or spin-electronic devices. In order to elucidate the electronic non-equilibrium in the surface layer of metal/semiconductor interfaces, it is indispensable to understand the transient state of photo-excited semiconductor surface. In this work, we have performed photoemission spectroscopy for Cr/GaAs(100) surface with the combinational use of synchrotron radiation and laser.

Experimental

Experiments were performed at BL5U. N-type (Si-doped, $3.0x10^{16}$ cm^{-3}) and p-type (Zn-doped, $3.0x10^{18}$ cm^{-3}) GaAs(100) wafers were used as the substrate. An As-capped GaAs(100) wafer was used as n-type substrate. An As capping layer was removed by heating the sample in the ultra-high vacuum. The clean surface of p-type substrate was obtained by the Ne^{+}-ion sputtering and annealing cycles. We used the mode-locked Ti:Sapphire laser (COHERENT Mira 900-F) which is synchronized with the synchrotron radiation in the multi-bunch operation. The time-resolved photoemission measurements in nano-second region were performed by the so-called pump-probe technique with the synchrotron radiation and laser. The laser light was transported to the viewport of the main experimental chamber using an optical fiber. The laser light was then focused onto the sample surface with a 3 mm radius spot. The spatial overlap of the laser with the synchrotron radiation was adjusted by eyes.

Results and Discussions

Figure 1 shows the Ga *3d* photoemission spectra with and without laser illumination measured at 80K. The delay time between laser and SR is 0 ns. The Cr coverage is also shown in the figure. These core-level spectra were deconvolved into bulk, surface and eventually reacted components, using a least-square curve fitting technique. The curve fitting parameters for Ga 3*d* (Lorentzian width, spin-orbit splitting, and branching ratio) were identical to those reported for GaAs(100) clean surface [1]. The Ga 3*d* peak is composed of one bulk and two surface components and reproduced well with same fitting parameters as those reported in Ref. 1. The bulk and surface components shift to 0.23 eV higher binding energies at the Cr deposition of 0.05 nm. This energy shift corresponds to the increase of the band-bending. The further deposition of Cr produces new reacted components at lower binding energy. At the Cr deposition of 0.5 nm, two reacted components are clearly observed at 0.76 and 1.02 eV lower binding energies than the bulk component. The spectral intensity of bulk component decrease with the Cr deposition and two surface components disappear at the Cr deposition of 0.2 nm.

As shown in Fig. 1, it is clearly seen that the peak position of the Ga *3d* spectrum is shifted to lower binding energy under the laser excitation. From the conjunction with our previous studies for GaAs(100) clean surface, we have concluded that the present core-level shift is originated from the surface photo-voltage (SPV) effect. It is found that the Ga 3*d* peak shows larger SPV shift than that for clean surface at the Cr deposition of 0.05 and 0.10 nm. A simple SPV formula derived from the depletion approximation scheme with excess photo-carriers suggests that the surface with larger band-bending shows larger SPV value. The Cr deposition, as mentioned above, leads the increase of the band-bending. Thus, the small amount of Cr deposition leads the increase of the SPV shift. On the other hand, the further depositions of Cr decrease the SPV shift, while the band-bending value is larger than that of clean surface. The SPV value also depends on amount of the photo-excited carriers. It is considered that the small SPV values at large Cr coverage is due to the lifetime of photo-excited carriers shorter than the pulse width of the probe light.

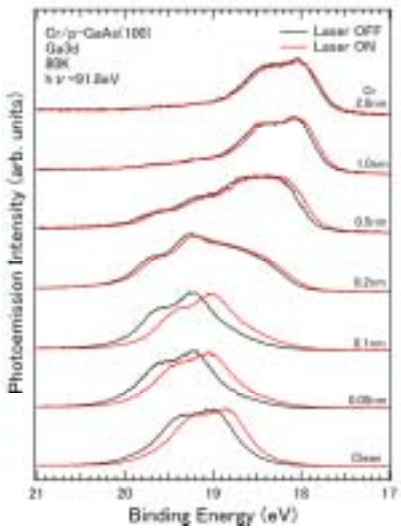

Fig. 1 Ga *3d* photoemission spectra with and without laser illumination.

[1] D. Mao *et al*., Phys. Rev. B **45** (1992) 1273.

BL5U

Photoelectron Spectroscopic Study of Fe Films on NEA Surface

N. Takahashi[1], S. Nakanishi[2], H. Itoh[2], S. Koshiba[2], T.-H. Shen[3], T. Zhang[4], S. Tanaka[5], K. Takahashi[6], M. Kamada[6]

[1]*Department of Physics, Kagawa University, Takamatsu 760-8522, Japan*
[2]*Department of Advanced Materials Science, Kagawa University, Takamatsu 761-0396, Japan*
[3]*Institute for Materials Research, University of Salford, Greater Manchester M5 4WT, UK*
[4]*Blackett Lab, Imperial College of Science, Technology and Medicine, London SW7 2BZ, UK*
[5]*Research Center for Materials Science, Nagoya University, Nagoya 464-8602, Japan*
[6]*Synchrotron Light Application Center, Saga University, Saga 840-8502, Japan*

NEA (negative electron affinity) semiconductors are used as efficient photocathodes, due to their high degrees of polarization and efficiency. However, from a fundamental science point of view, the details of NEA formation are not fully understood [1]. On the other hand, the study of magnetic thin films on semiconductor substrates has been widely carried out due to the applicability to magneto-electronics devices, such as the Spin Polarised Field Effect Transistor [2]. As a typical basis for such devices, the Fe/GaAs system has been extensively studied for decades [3] because of its great promise in the possible use of hybrid ferromagnetic metal-semiconductor structures for applications. In this report, we present a study of a Fe covered NEA.

Experiment

All experiments were carried out at RT in UHV chamber with the base pressure of about 3×10^{-8} Pa. A Zn doped (1×10^{19} atoms/cm^3) p-GaAs(100) wafer with (8×2) surface reconstruction was used as a substrate. The NEA intensity was measured as the absolute value of the photocurrent from the biased (-10 V) sample while the He-Ne laser was on and off. Fe was deposited on the NEA surface a total of 5 times, yielding estimated coverages of 9.7 (after the first Fe deposition, Fe#1), 29 (Fe#2), 68 (Fe#3), 97 (Fe#4) and 115 Å (Fe#5). Photoelectron spectroscopy was carried by using 100 eV.

Results and Discussion

The relative NEA intensity is shown in Figure 1 as a function of Fe coverage and is compared with the lowering of the work function. The intensity is kept at 50, 20 and 7 % of the maximum intensity obtained from the pure NEA surface after Fe depositions Fe#1, #2 and #3, respectively. The intensity decreases with increasing coverage, although the work function is almost constant even at thicker coverages. This is in good agreement with the literature [1] which suggests that the band bending is not a sufficient condition for the amplitude of the NEA effect.

Figure 2 shows normalized core peaks from (a) Cs 4*d*, (b) As 3*d* and (c) Ga 3*d* levels. Spectra from the bottom to the top of each panel indicate different stages of Fe growth (layers Fe#1 and Fe#2, respectively) after NEA treatment. The Cs 4*d* and Ga 3*d* peaks shift to higher kinetic energies, and a new component is seen to grow at the lower energy side of the As 3*d* peak. The Ga 3*d* peak appears to obtain a higher energy side component whilst losing a lower side one. Moreover, the width of the Cs 4*d* peak was found to decrease.

It was found that the Fe covered surface still has NEA characteristics which is comparable to the standard NEA, even in the thicker Fe coverage region of about 100 Å. Furthermore, the change of NEA intensity appears to be independent of the change of the work function. The core level peak results imply that the overlayer has a complicated structure, dependent on its depth from the top of the layer.

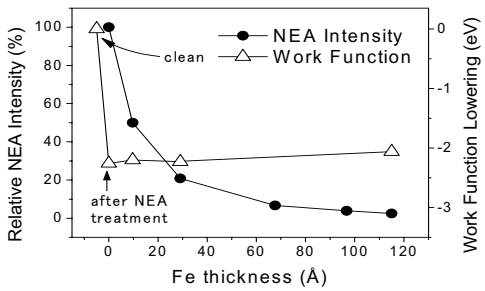

Fig. 1 The variation of the relative NEA intensity and the relative work function lowering of the sample.

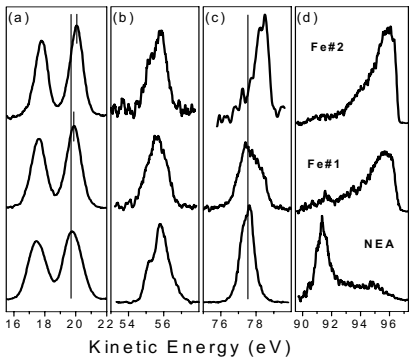

Fig. 2 Panel (a), (b) and (c) show core peaks from Cs 4*d*, As 3*d* and Ga 3*d* levels, respectively. Panel (d) is the VB.

[1] ex, S. Moré *et al.*, Surface Science **527** (2002) 41.
[2] S. Datta and B. Das, Appl. Phys. Lett. **56** (1990) 665.
[3] J. Shen *et al.*, Surface Science **500** (2002) 300.

BL5U

Electronic Structure of Relevant Crystals of Bulk Metallic Glasses

T. Takeuchi[1], S. Nakano[2], T. Kondo[2], T. Kitao[2], T. Ito[3], S. Kimura[3]
[1]*EcoTopia Science Institute, Nagoya University, Nagoya 464-8603 Japan*
[2]*Department of Crystalline Materials Science, Nagoya University, Nagoya 464-8603 Japan*
[3]*Institute for Molecular Science, Okazaki 444-8585 Japan*

Amorphous metals are generally produced by rapidly solidification techniques, such as liquid quenching and vapor deposition methods. These techniques restrict the sample shape to ribbons or thin films. Recently, however, formation of amorphous metals without rapidly quenching was reported for Zr-based, Fe-based, and Pd-based alloy systems, and amorphous metals with bulk shape of nearly ten centimeter in dimension had been produced. Since amorphous phase are characterized by high mechanical strength and extremely soft magnetic properties, amorphous phase with bulk shape encourages us to utilize it in a large number of applications. Unfortunately, however, guiding principles to produce "stable" amorphous phases and to control their physical properties have not been well understood yet. In order to utilize them in many applications, it is highly requited to investigate their "stabilization" mechanism.

To gain deep insight into the origin of their stabilization mechanism, we have to evaluate the free energy of the bulk amorphous phases. Internal energy and entropy should be equally taken into account to estimate the free energy of the amorphous, whereas the crystalline phases are stabilized dominantly by the contribution of the internal energy. If the covalent bonds associated with *d*-orbital of the constituent transition-metal elements reduce the internal energy of the relevant crystals, local atomic arrangements (clusters) in the crystals especially around the transition metal elements should be regarded as the most important factor for the phase stabilization. This consideration lets us strongly believe that the local atomic clusters in the relevant crystals exist also in the corresponding amorphous phase, and their random arrangements leads to sufficient reduction in the free energy both by the low internal energy and the large entropy.

In order to confirm validity of this idea, we analyzed the local atomic clusters in the relevant crystals of the Zr-Ni-Al amorphous phase. As the simplest approximation, all coordination polyhedra centered at a Zr atom in the crystalline phases are picked up. Their compositions are calculated by assuming that the surrounding atoms supply $1/Z$ of single element, where Z is the coordination number of the surrounding atom. We found as a result of this analysis that the composition of the most "stable" amorphous phase is surrounded by compositions of the local atomic clusters of the relevant crystals. The entropy associated with the random arrangement of the clusters was calculated on the basis of the well-known Bragg-Williams approximation. The resulting entropy possess its maximum value in the vicinity of the composition for the largest $\Delta T_x = T_x - T_g$, where T_x and T_x represent crystallization temperature and glass-transform temperature of the amorphous phase, respectively. This result strongly suggests the crucial role of the entropy in reducing free-energy of the bulk amorphous phases.

The internal energy associated with covalent orbital was investigated using the DXVα cluster calculation. The validity of the resulting energy levels was confirmed by the high high-resolution photoemission spectroscopy, HRPES. HRPES measurements were carried out in the BL5U of the UVSOR, Okazaki. The incident photon energy was selected to be 20 ~ 40 eV, with which high-flux and high-energy resolution of ΔE ~ 20 meV are simultaneously obtained.

We confirmed that the calculated cluster levels associated with *d*-orbital of the Zr atoms reproduce well the energy levels of the *d*-orbital measured by the HRPES. From the calculated cluster levels, total energy of the clusters was quantitatively evaluated. We confirmed that the difference of the internal energy among the all clusters stays within the energy scale of ST at T_x ~ 700 K.

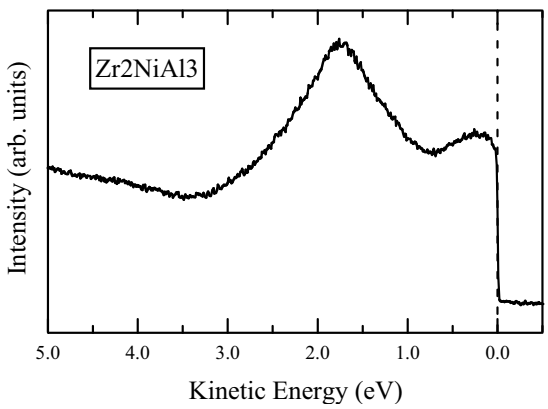

Fig. 1 HRPES spectrum of the Zr_2NiAl_3 with hν = 20 eV at 20 K. Two peaks centered at 1.8 eV and 0.3 eV correspond to the Ni 3*d* and Zr 4*d* orbitals, respectively. Widely extending *d*-orbitals are brought about by the hybridization of *d*-orbitals with *s*,*p*-orbitals of the surrounding elements.

BL5U

Surface-Passivant Dependence of Photoemission Spectra of Alkanethiolate-Passivated Au Nanoparticles on the HOPG Substrates

A. Tanaka[1], M. Imamura[1,2], R. Saito[1,2]
[1]*Department of Mechanical Engineering, Kobe University, Kobe 657-8501, Japan*
[2]*Department of Physics, Tohoku University, Sendai 980-8578, Japan*

The chemically synthesized metallic nanoparticles surface-passivated by various organic molecules are attracting much interest from the viewpoints of both fundamental and device physics, since they show the distinctive physical and chemical properties found in neither bulk nor molecular/atomic systems. In order to develop the future nanostructured devices using these organic-inorganic hybrid nanoparticles, it is especially indispensable to understand the interface features as well as their electronic structures. In this work, we have carried out a systematic photoemission study of alkanethiolate- (AT-) passivated Au nanoparticles on the HOPG substrates in order to characterize their interface features.

The synthesis procedure of AT-passivated Au nanoparticles is described elsewhere [1]. We have used the octanethiol ($C_8H_{17}SH$, OT), dodecanethiol ($C_{12}H_{25}SH$, DT), and hexadecanethiol ($C_{16}H_{33}SH$, HDT) as the surface-passivants of AT molecules. Photoemission measurements were performed at BL5U of UVSOR Facility. Photoemission measurements were performed with the incident photon energy of 190 eV at room temperature. Further ultraviolet photoemission measurements with the He I resonance line ($h\nu$ = 21.2 eV) as the excitation source were performed at Kobe University.

From the low-energy cutoff of the ultraviolet photoemission spectrum due to the vacuum level measured with He I resonance line (not give here), it is found that the effective work functions of the present all AT-passivated Au nanoparticles with mean diameters of 4 nm are smaller than bulk Au crystallite. Moreover, these effective work functions are smaller than the previously reported ones of self-assembled monolayers of AT molecules on the Au surfaces [2], and exhibit no surface-passivant dependence. This change in the surface potential is considered to originate from the interface dipoles formation at AT molecules-Au nanoparticle heterojunction. These interface dipoles are considered to be composed of the intrinsic dipoles of AT molecules (dipole moment of the hydrocarbon tail region) and the dipoles induced by charge transfer due to the Au-S chemical bonds formation. In order to characterize the bonding nature at the interface between AT molecules and Au nanoparticle surface, we have performed the Au 4*f* core-level photoemission measurements as shown in Fig. 1. As previously reported [2, 3], Au 4*f* core-level spectra of AT-passivated Au nanoparticles consist of two components. The components with lower binding energy (blue lines in Fig. 1) and higher binding energy (red lines in Fig. 1) originate from the inner Au atoms of Au nanoparticles (bulk component) and the surface Au atoms of Au nanoparticles bonded to surface-passivants of AT molecules (surface component), respectively. As shown in Fig. 1, the chemical shifts of the surface components relative to the bulk components are almost same among the present AT-passivated Au nanoparticles. This indicates that the charge transfer between the surface passivants of AT molecules and Au nanoparticle surfaces and the resultant dipoles are almost same among the present AT-passivated Au nanoparticles. Therefore, the intrinsic dipoles of AT molecules dominate the dependence of effective work function on the surface-passivant molecules, and are almost same among the present AT-passivated Au nanoparticles.

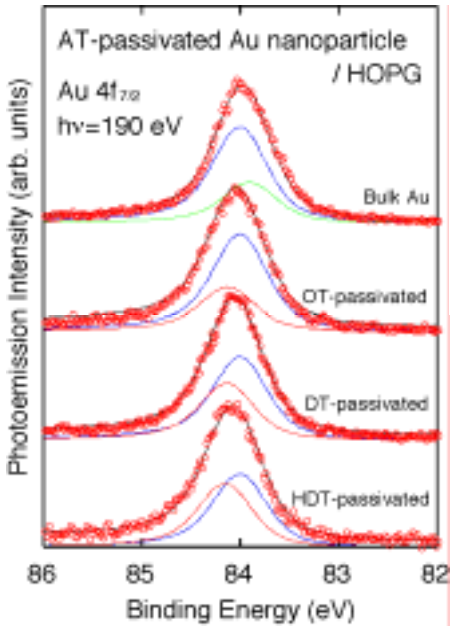

Fig. 1 Au $4f_{7/2}$ core-level photoemission spectra of various AT-passivated Au nanoparticles with mean diameter of 4 nm on the HOPG substrates bulk Au polycrystalline film for a comparison.

[1] M. Imamura and A. Tanaka, submitted.
[2] D. M. Alloway, M. Hofmann, D. L. Smith, N. E. Gruhn, A. L. Graham, R. Colorado, Jr., V. H. Wysocki, T. R. Lee, P. A. Lee, and N. R. Armstrong, J. Phys. Chem. B **107** (2003) 11690.
[3] A. Tanaka, Y. Takeda, T. Nagasawa, and K. Takahashi, Solid State Commun. **126** (2003) 191.
[4] A. Tanaka, Y. Takeda, M. Imamura, and S. Sato, Phys. Rev. B **68** (2003) 195415.

BL5B

Desorption of Ionized Clusters from Water Physisorbed on Solid Neon

T. Tachibana[1], Y. Yamauchi[1], T. Miura[1], T. Hirayama[2], M. Sakurai[3], I. Arakawa[1]
[1]*Dept. Phys., Gakushuin Univ., Mejiro, Toshima, Tokyo 171-8588, Japan*
[2]*Dept. Phys., Rikkyo Univ., Nishiikebukuro, Tokyo 171-8501, Japan*
[3]*Dept. Phys., Kobe Univ., Rokkodai, Nada, Kobe 657-8501, Japan*

There has been a growing interest in the properties of ice surface and ice particle for both fundamental and practical points of view in the field of surface, environmental and planetary sciences. Understanding electronic excitations and relaxation processes of water molecule is one of the most important subjects in these fields. A variety of studies have been made on electron- and photon-stimulated desorption (ESD/PSD) at ice surface [1, 2].

We have investigated the PSD of $(H_2O)_nH^+$ from water physisorbed on solid Ne. From the measurements of the desorption yield as a function of the incident photon energy, the desorption of $(H_2O)_nH^+$ is effectively and indirectly induced by the multiple-excitation and -ionization of rare gas substrates. The direct excitation of the water molecule does not induce noticeable desorption of $(H_2O)_nH^+$.

The PSD-experiments have been carried out in an ultra high vacuum system at the beam line 5B at UVSOR in Institute for Molecular Science, Okazaki. The mass spectrum of PSD ions was measured by a time-of-flight (TOF) technique. The desorption yield was normalized by the light intensity, which was continuously monitored by the photoemission current from a gold-plated mesh inserted in the beam lines. The sample film was prepared on a Pt(111) substrate, which was fixed to a liquid He cryostat and cooled down to 6 K. The sample was irradiated by the photon in the energy range between 6 and 1000 eV. The incident angle of the photon beam was 20 deg from the normal.

Photodesorption yield of $(H_2O)_nH^+$ [n = 2 - 5] from water adsorbed on Ne substrate in the 38 - 100 eV photon energy is shown in Fig. 1. The desorption yield increases gradually from 60 eV to 90 eV of the excitation energy. The threshold of ESD $(H_2O)_nH^+$ from ice surface was reported at 70 eV [1], however we have not observed the threshold-like increase of the yield near 70 eV excitation energy. The increase of $(H_2O)_nH^+$ desorption yield above 60 eV is probably related to direct double photoionization of Ne because the threshold energy is reported at 62.5 eV in the gas phase [3]. This result leads us to the conclusion that the desorption of $(H_2O)_nH^+$ is caused by the multiple-hole states of the rare gas substrates.

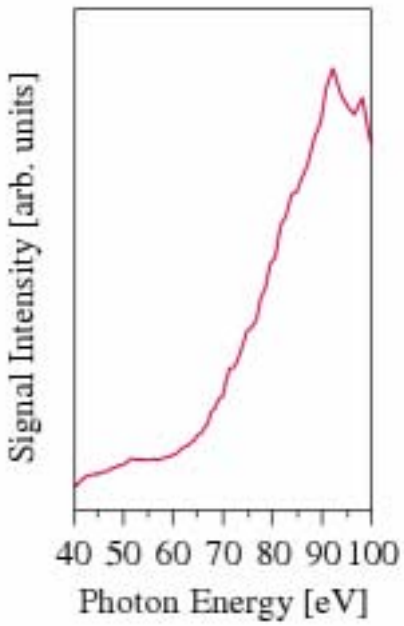

Fig. 1 $(H_2O)_nH^+$ desorption yield [n = 2 - 5] as a function of the incident photon energy from water (0.2 ML) on solid Ne (100 ML) in the 40 - 90 eV energy range at 6 K of the sample temperature.

[1] J. Herring, A. Aleksandrov, and T. M. Orlando, Phys. Rev. Lett. **92** (2004) 187602.
[2] R. Rosenberg, V. Rehn, V. Jones, and A. Green, Chem. Phys. Lett. **15** (1981) 488
[3] R. Bartlett and P. J. Walsh, Phys. Rev. A **46** (1992) 5547.

BL8B1

Characterization of Carbon-Based Material Formed by Focused-Ion-Beam Chemical-Vapor-Deposition

K. Kanda, J. Igaki, Y. Kato, R. Kometani, S. Matsui

University of Hyogo, Laboratory of Advanced Science and Technology for Industry, Kamigori, Hyogo, 678-1205 Japan

Nano-structure fabrication using focused ion beam-chemical vapor deposition (FIB-CVD) has been achieved in view of the production of the numerous three-dimensional nano-tools [1]. The nano-structural material formed by FIB-CVD was considered to be composed of the carbon-based material, however the structural properties has not been sufficiently understood. In the present study, we will show that the combination of Raman spectroscopy, near-edge x-ray absorption fine structure (NEXAFS) spectroscopy and other analyses can provide useful information on the structure of carbon-based material formed by FIB-CVD method.

The NEXAFS measurement was performed at the BL8B1 stage of UVSOR in the Institute for Molecular Science. The synchrotron radiation provided by the 0.75 GeV electron storage ring was dispersed by a constant-deviation constant-length spherical grating monochromator and was perpendicularly irradiated to the sample film surface. The NEXAFS C *K*-edge spectra were measured in the energy range 275-320 eV with 0.5 eV FWHM resolution. The detection of electrons coming from sample was performed in the total electron yield (TEY) mode. The intensity of the incident photon beams I_0 was measured by monitoring the photocurrent from a gold film. The absorption signal was given by the ratio between the out-coming electron intensity from the sample I_s and the intensity from the gold film, I_0.

Figure 1 depicts the NEXAFS carbon *K*-edge spectrum of carbon material formed by 30 kV Ga^+ FIB-CVD using *Phenanthrene* as a source gas. For comparison, the spectra of commercial diamond-like-carbon (DLC) produced by ion-plating (IP) method and graphite are also depicted in the figure. NEXAFS was useable for the characterization of amorphous carbon materials [2]. Resonance peaks of 291.9 and 292.8 eV, which are characteristic of graphite, are not observed in the NEXAFS spectrum of FIB-CVD DLC. The peaks at 295.1 eV and 297.8 eV are assignable to resonance peaks to the σ* states from 1*s* level of carbon atom neighboring Ga atoms, which are residue from ion beam. A resonance at about 285.4 eV is due to transitions from C 1*s* level to unoccupied π* states of sp^2 (C=C) sites. The sp^2 content of the DLC films formed by FIB-CVD method is smaller than that of the IP DLC film. This result is consistent with that the hardness measurement of the FIB-CVD DLC (67 GPa) and IP DLC (26 GPa). As the result, FIB-CVD method can construct ultra-hard structure, because the deposited material by this method is DLC with a high content of sp^3 hybridized carbon.

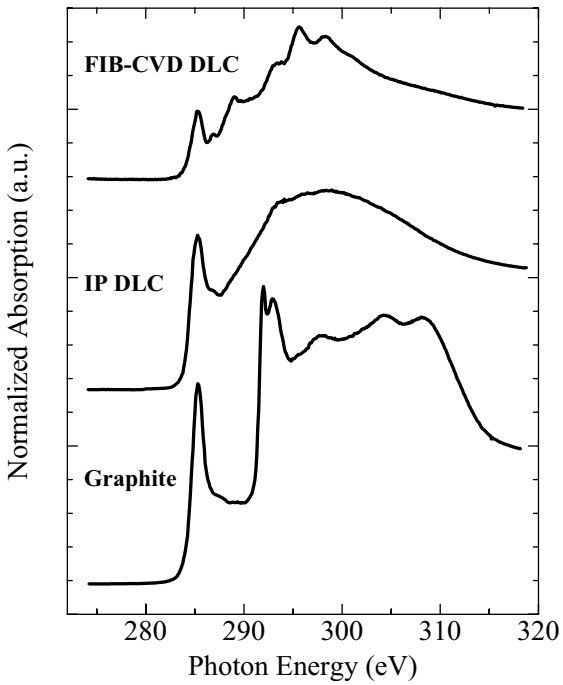

Fig. 1 NEXAFS spectra in the C *K*-edge of FIB-FVD DLC, IP DLC and graphite: The pre-edge resonance at 285.4 eV is due to the C 1*s* → π* transitions. The broad band between 290 and 310 eV is the result of overlapping C 1*s* level to σ* unoccupied states of *sp*, sp^2 and sp^3 sites. The sharp peak at 295.1 and 297.8 eV at the spectrum of FIB-CVD DLC are assignable to 1*s* → π* transitions of carbon atom neighboring Ga atom.

[1] R. Kometani *et al.*, Jpn. J. Appl. Phys. **42** (2003) 4107.
[2] K. Kanda *et al.*, Nucl. Inst. Meth. B **206** (2003) 880.

BL8B1

N *K* XAFS Analysis of Some Porphyrin Compounds and Their Complexes

H. Yamashige[1], T. Kurisaki[1], H. Wakita[1,2]

[1]*Department of Chemistry, Faculty of Science, Fukuoka University, Nanakuma, Jonan-ku, Fukuoka 814-0180, Japan*

[2]*Advanced Materials Institute, Fukuoka University, Nanakuma, Jonan-ku, Fukuoka 814-0180, Japan*

Metalloporphyrins, used as biomimetic catalysts, are important prosthetic groups in enzymes, and offer the potential for substrate oxidation[1]. Iron-porphyrins, in particular, have been used as cytochrome P-450 models for oxidative catalysis using a large variety of oxygen donors, such as iodosylbenzene and hydrogen peroxide. The introduction of electron-withdrawing substitutes at the *meso*-positions of Fe-porphyrin complexes affects the catalytic activity of the oxidation reaction for cytotoxin and pollution hazards. The chemical state of Fe ions in Fe-porphyrin complexes with *meso*-substitutes has been examined using IR, XRD, NMR, EPR, Mössbauer, electron spectroscopy, MD, and DFT calculations. Notwithstanding, it remains unclear how the influence of electron-withdrawal is transmitted to the electron state of the center Fe ion in each Fe-porphyrin complex. Elucidation of the electron structure throughout a Fe-porphyrin complex with *meso*-substitutes is an important task toward the development of stable and highly active Fe-porphyrin complexes as oxidation catalysts.

X-ray absorption spectra of near C and N *K* absorption edges were (XAFS) measured at BL8B1 of the UVSOR in the Institute of Molecular Science, Okazaki [2]. The energy of the UVSOR storage ring was 750 MeV and the stored current was 110-230 mA. The absorption was monitored by the total electron yield using a photomultiplier. The C and N *K* XANES spectra for tetraphenylporphyrin (TPP) are shown in Fig. 1 and Fig. 2. The peaks which appeared at approximately 282, 285, 395, 398, 400, and 405 eV in each experimental spectrum are labeled A, B, C, D, E, and F in the order of increasing energy. This work is to examine electron structures of TPP, TCPP, and TSPP using crosschecks of XANES data for C and N *K* absorption edges in combination with DV-Xα MO calculations. These results indicated that a *p*-electron-withdrawing group on the phenyl group in porphyrin compounds engenders a unique electron state because of the electron-withdrawal strength itself.

Crosschecks of XANES data for multi-element absorption edges are important not only for porphyrin compounds and complexes, but also for other numerous metal complexes, especially those with a layer structure or chain structure, because they are closely related to intermolecular interaction of electrons. This method is applicable to the design and development of new metal complexes with a useful function by obtaining detailed information about the electronic structure along with an electron state calculation method, such as the DV-Xα MO method. An experimental setup of simultaneous measurements of XANES, which we are currently constructing for the laboratory users, will facilitate such studies.

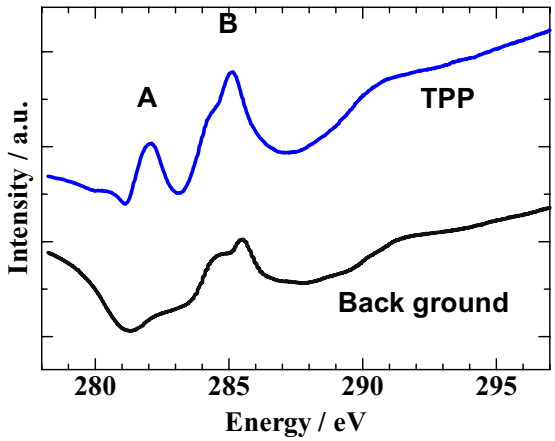

Fig. 1 C *K* XANES spectra of TPP.

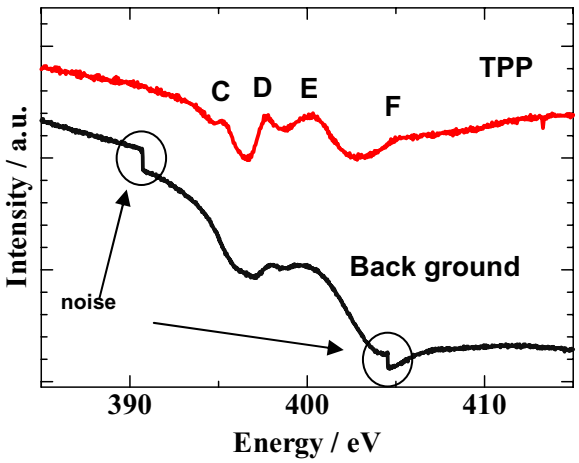

Fig. 2 N *K* XANES spectra of TPP.

[1] J. H. Chou, H. S. Nalwa, and M. E. Kosal, *The Porphyrin Handbook* vol. **7**, ed. K. M. Kadish, K. M. Smith, R. Guilard (Academic Press, San Diego, CA, 2000) 41.

[2] S. Murata, T. Matsukawa, S. Naoè, T. Horigome, O. Matsuodo, and M. Watanabe, Rev. Sci. Instrum. **63** (1992) 1309.

BL8B2

Ultraviolet Photoelectron Spectra of Three Tm@C_{82} Isomers

S. Hino[1,2], N. Wanita[2], K. Iwasaki[1], D. Yoshimura[3,4], N. Ozawa[5], T. Kodama[5], K. Sakaguchi[5], H. Nishikawa[5], I. Ikemoto[5], K. Kikuchi[5]

[1]*Faculty of Engineering, Chiba University, Chiba 263-8522, Japan*

[2]*Graduate School of Science & Technology, Chiba University, Chiba 263-8522, Japan*

[3]*UVSOR, Institute for Molecular Science, Okazaki 444-8585, Japan*

[4]*Research Center of Material Science, Nagoya University, Nagoya 464-8602, Japan*

[5]*Department of Chemistry, Tokyo Metropolitan University, Tokyo 192-0397, Japan*

Abstract

Ultraviolet photoelectron spectra (UPS) of three Tm@C_{82} isomers were measured with a synchrotron radiation light source. The upper valence band spectra (0 – 5 eV) of three isomers are different each other and they also differ from those of other trivalent metal atoms encapsulated metallofullerenes such as La@C_{82}, Sc@C_{82} and Gd@C_{82}. Resemblance of the spectra of Tm@C_{82} (II) and Ca@C_{82} (III) suggests identical cage structures of these two metallofullerenes. The UPS are well reproduced by simulated spectra obtained with *ab initio* calculation, which indicates that isomers I – III have C_s (No. 4), C_2 (No. 5) and C_{2v} (No. 9) cage structures.

Results and Discussion

The spectral onsets of the UPS of three Tm@C_{82} isomers (I) – (III) are 0.85, 0.75 and 0.9 eV, respectively, which is relatively large compared with those of La@C_{82} [1] and Gd@C_{82} [2] but almost the same as those of Ca@C_{82} isomers [3]. This finding is closely related to the amounts of transferred electrons from encapsulated metal atom to the fullerene cage.

The spectra obtained with 40 eV photon energy show upper valence band very distinctly. As explicit difference among the spectra lies mainly in the upper valence band region (pseudo π-electron region) so that 40 eV UPS of three Tm@C_{82} isomers are shown in Fig. 1 for comparison. As for the deeper valence band (mainly due to pseudo σ-electrons) region there is hardly any difference among the three Tm@C_{82} spectra. This implies that electronic structures of skeletal cage structures of three isomers are not so different. As for the upper valence band region the situation is quite different. Although onset positions of these spectra do not change so much, the first structure of each spectrum differs so much. Intensity ratio of second and third structures of these spectra also differs. The UPS of two Ca@C_{82} isomers are also shown in Fig. 1. The UPS of Tm@C_{82} (II) and Ca@C_{82} (III) are essentially the same which indicates that these two metallofullerenes have the same electronic structure derived from the same cage structure.

The NMR analysis suggests symmetry of three Tm@C_{82} isomers are C_s, C_2 and C_{2v}, respectively. There are nine isolated pentagon rule (IPR) satisfying cages for C_{82}. There is only one C_{2v} cage among them so that cage structure of isomer III can be determined exactly to be C_{2v} (No. 9). There are three C_s and C_2 cages for IPR satisfying C_{82} cage. The NMR could not elucidate the exact cage structure for isomers I and II. The UPS of three isomers can be well reproduced by simulated spectra obtained with *ab initio* calculation assuming C_s (No. 4), C_2 (No. 5) and C_{2v} (No. 9) cage structures. Thus, cage structures of three isomers can be determined [4].

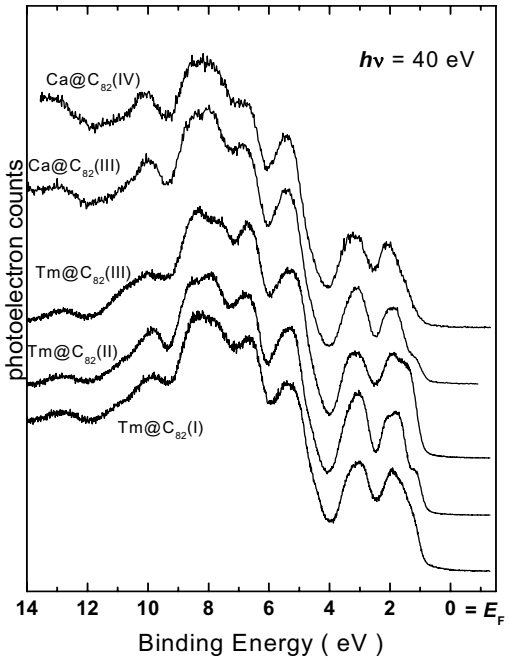

Fig. 1 The UPS of three Tm@C_{82} isomers and two Ca@C_{82} isomers.

[1] S. Hino *et al*., Phys. Rev. Lett. **71** (1993) 4261.
[2] S. Hino *et al*., Chem. Phys. Letts. **281** (1997) 115.
[3] S. Hino *et al*., Chem. Phys. Lett. **337** (2001) 165.
[4] S. Hino *et al*., Chem. Phys. Lett. **402** (2004) 217.

BL8B2

Epitaxial Growth of Copper Tatrakis(Thiadiazole)Porphyrazine Film

K. Kanai[1], E. Kawabe[1], D. Yoshimura[2], Y. Suzuki[1], M. Fujimori[1], H. Yoshikawa[1], K. Awaga[1], K. Seki[1,2,3]

[1]*Graduate School of Chemistry, Nagoya University, Nagoya, 464-8602 Japan*
[2]*Research Center for Material Science, Nagoya University, Nagoya, 464-8602 Japan*
[3]*Institute for Advanced Research, Nagoya University, Nagoya, 464-8602 Japan*

Introduction

Thin films of organic semiconductors have been attracting much interest over the past decade for their potential technological applications. In organic devices, such as organic field effect transistor and organic light emitting diode, charge transport and luminescence properties are strongly affected by the structural properties of the films. Thus, it is important to understand the mechanism of molecular aggregation, packing, and orientation to control the structure of the film for improvement of the properties of such devices.

In this research, we focus on the epitaxial growth of phthalocyanine-based molecules, copper tetrakis -(thiadiazole)porphyrazine (CuTTDPz) film on GeS(100) surface. CuTTDPz is expected to have stronger inter-molecule interaction than that of phthalocyanine because of the close contact between the sulfur and nitrogen atoms of the thiadiazole group [1]. Comparison between CuTTDPz film and other phthalocyanine film will provide insight into the role of inter-molecule interaction on epitaxial growth of organic thin films.

Experimental

Low energy electron diffraction (LEED) was performed to study the arrangement of CuTTDPz molecules on GeS(100) surface. Angle-resolved ultraviolet photoemission spectroscopy (ARUPS) was performed to determine the molecular orientation of CuTTDPz molecule on GeS(100) surface. ARUPS experiment was done in UVSOR-II BL8B2 with VG-CLAM4 analyzer. Clean GeS(100) surface was obtained by cleaving the surface of GeS single crystal under ultrahigh vacuum condition. The film of CuTTDPz was in situ evaporated onto clean GeS(100) surface.

Results and Discussion

Clear diffraction spots from CuTTDPz molecules shown in Fig. 1 indicate epitaxial growth of CuTTDPz molecules deposited on GeS(001) surface. From this result, the unit cell of CuTTDPz film on GeS(100) surface is estimated to be twice as large as that of ZnPc.[2]

Figure 2 shows the take-off angle θ dependence of ARUPS spectra of CuTTDPz film deposited on GeS(001) surface. The inset gives the measurement geometry. ARUPS spectra show strong dependence on θ, especially in HOMO, indicating that CuTTDPz molecules have preferred orientation on the GeS(100) surface. From comparison between the observed θ dependence of ARUPS spectra and theoretical calculation by independent atomic center approximation, CuTTDPz molecule is found to be almost flatly lying. The role of intermolecular interaction for both molecular arrangement and orientation will be discussed near future.

Fig. 1 LEED pattern of CuTTDPz film deposited on GeS(001) surface. Primary energy is 40 eV and the thickness of the film is 0.4 nm. The black circles in the figure represent diffraction spots from GeS(100).

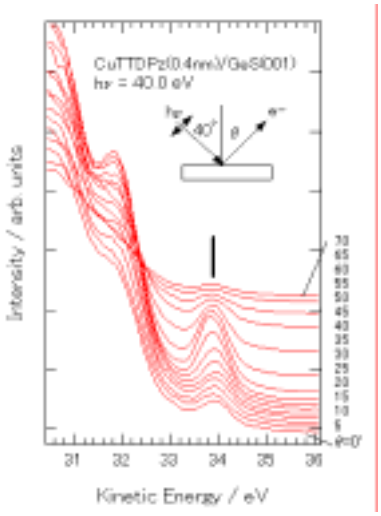

Fig. 2 ARUPS spectra of CuTTDPz film deposited on GeS(100) surface. Vertical bar points at the highest occupied molecular orbital (HOMO) CuTTDPz.

[1] Y. Suzuki, *et al*, Chem. Eur. J. **10** (2004) 5158.
[2] E. Kawabe, unpublished.

BL8B2

Angle-Resolved UV Photoelectron Spectra of OTi-Phthalocyanine Monolayer on Graphite

S. Kera[1,2], H. Yamane[1], H. Fukagawa[1], T. Hanatani[1], M. Ono[1], S. Nagamatsu[1], T. Yokoyama[1], D. Yoshimura[3], K. K. Okudaira[1], K. Seki[2], N. Ueno[1]

[1]*Faculty of Engineering, Chiba University, Chiba 263-8522 Japan*

[2]*Institute for Molecular Science, Okazaki 444-8585 Japan*

[3]*Research Center for Materials Science, Nagoya University, Nagoya 464-8602 Japan*

A few years ago, we succeeded to observe a very sharp HOMO band with clear vibration satellites on a well-ordered Cu-phthalocyanine (Pc) on graphite [1]. After detecting the highly-resolved HOMO band, we could discuss the complex nature of band width, shape and position in organic solid systems [1-3].

Very recently, we observed peculiar angular distribution for OTiPc doublelayer/graphite system. It may be related to a photoelectron scattering process passing through a different local potential within the film. Photoelectron angular distribution involves information on the initial wavefunction, and thus the quantitative analysis of the angular distribution provides a detailed origin of the UPS bands, as well as a geometrical structure of organic thin films [4]. In this work, we measured take-off angle dependencies of angle-resolved UPS (ARUPS) for well-defined OTiPc monolayer precisely.

Experiments

ARUPS spectra were measured at photon incidence angle α = 70°, hν = 20 eV, and T = 295 K. θ dependence of ARUPS spectra was analyzed using the single-scattering approximation combined with molecular orbital calculation (SS/MO) [4,5]. The purified OTiPc was carefully evaporated onto the HOPG. Characterization of the film growth of the OTiPc/graphite has been carried out [6]. Coverage of the film can be estimated from the total shift of the vacuum level as discussed in the previous paper [3]. To obtain the well-ordered monolayer film, subsequent annealing is performed at 420 K/2 h.

Results and Discussion

Figure 1(a) shows θ dependence of ARUPS of OTiPc monolayer (annealed-0.8-MLE) on HOPG surface. The intensity is normalized to the incidence photon flux and the background is subtracted. The HOMO band is assigned to a single π MO as in other Pcs (inset of Fig. 1) [1-3]. Very sharp asymmetric HOMO bands are detected for all photoelectron-take-off-angles (θ = 0 ~ 60°).

Figure 1(b) shows the comparison between observed and calculated θ dependences of the HOMO-band intensities with the SS/MO (HF/STO-6G) for the molecular tilt angle β = 0°, which gave the best agreement with the observed θ pattern. It indicates that the OTiPc molecules orient flat to the HOPG surface with O-atom protruding the vacuum as illustrated in Fig. 1(b). Moreover, we found that effects of a multiple scattering are negligibly small for organic molecule, since our SS/MO approximation is applicable well even for the low-energy photoelectron (~ 15 eV).

Now to compare impacts on a different local potential, further experiments on the photoelectron angular distribution both for the monolayer and the doublelayer are in progress with theoretical calculations.

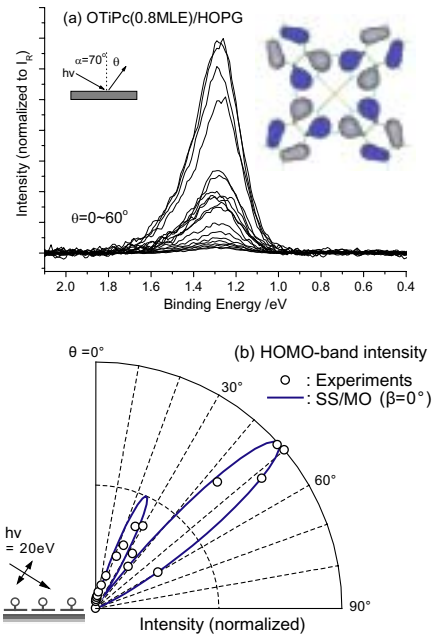

Fig. 1 (a) Take-off angle (θ) dependence of the ARUPS of the 0.8-MLE-OTiPc on HOPG(0001). The HOMO distribution of OTiPc is also shown. (b) Comparison between observed and calculated θ dependencies of the HOMO-band intensities with SS/MO approximation for hν = 20 eV and θ = 0°.

[1] S. Kera *et al.*, Chem. Phys. Lett. **364** (2002) 93.
[2] H. Yamane *et al.*, J. Electron Spectrosc. Relat. Phenom. **137-140** (2004) 223.
[3] There are some articles by us in IPAP conference proceedings, in press.
[4] N. Ueno *et al.*, J. Chem. Phys. **107** (1997) 2079.
[5] K. K. Okudaira *et al.*, J. Appl. Phys. **85** (1999) 6453.
[6] S. Kera et al,: Jpn. J. Appl. Phys. **40** (2001) 783.

BL8B2

Electronic Structure of $LiNi_{1-x}M_xO_2$ Mixed Oxides (I)

T. Miyazaki[1], H. Takeno[1], D. Yoshimura[2], T. Yamaguchi[1]

[1]*Department of Applied Chemistry, Faculty of Engneering, Ehime University, Matsuyama 790-8577 Japan*

[2]*Research Center for Materials Science, Nagoya University, Nagoya 464-8602, Japan*

An application of $LiNiO_2$ has been studied as a positive electrode of lithium secondary battery on the basis of the lamellar structure. And, the structure was maintained to over 1073 K under the oxidative atmosphere. It was reported that the surface lattice oxygen of $LiNiO_2$ had the catalytic property at around 1000 K for the oxidative coupling of methane [1]. Ultraviolet photoelectron spectroscopy was applied in order to discern the correlation of catalytic property and electronic states near the top of the valence band region. The valence band usually determines the electronic properties and the catalytic activities of the materials, therefore, it should be carefully investigated. At this approach, ultraviolet photoelectron spectra were measured as samples of $LiNiO_2$, $LiCoO_2$ and $LiNi_{1-x}M_xO_2$ (M = Mn, Ti, Al) were replaced with other metallic element a part of Ni site in $LiNiO_2$. Then, the electronic structure was examined from the incident photon energy dependence of ultraviolet photoelectron spectra in order to clarify the origin of selective catalysis and electronic properties.

$LiNiO_2$, $LiCoO_2$ and $LiNi_{1-x}M_xO_2$ (M = Ti, Al, Mn; x = 0.1) were prepared from $LiNO_3$, $Ni(OH)_2$ and $M(NO_3)_2$ by the solid-state reaction. The UPS spectra were measured using the angle resolved photoelectron spectroscopy equipment at BL8B2. The UPS spectra were measured for electrons emitted normal to the sample surface with an incident angle 45° of the light beam. The Fermi energy of the UPS system was determined by using the Fermi edge of gold films. A pure processing by Ar^+ sputtering or the heating of infrared radiation was carried out as a surface pretreatment of these samples.

Figure 1 shows the UPS spectra of $LiNiO_2$, $LiCoO_2$, $LiNi_{0.9}Mn_{0.1}O_2$, $LiNi_{0.9}Ti_{0.1}O_2$ and $LiNi_{0.9}Al_{0.1}O_2$ at 60 eV of the incident photon energy. These spectra were measured with reference to E_F as the zero of the energy scale. Several structures, denoted by the characters A－E, are observed at E_b = 1.6, 3.0, 4.9, 6.1 and 9.8 eV in the spectrum of $LiNiO_2$. The structure located at E_b = 3.0 eV of $LiNiO_2$, observed clearly in this study. In case of $LiCoO_2$, there were four structures on the top of the valence band. However, the B band was not clearly observed in those of $LiCoO_2$. Also, each band may be shifting to the high energy side of 0.5 ～ 1.0 eV. The UPS spectra of $LiNi_{0.9}Mn_{0.1}O_2$, $LiNi_{0.9}Ti_{0.1}O_2$, and $LiNi_{0.9}Al_{0.1}O_2$, a part of Ni site were replaced with Mn, Ti, and Al, have been composed of five bands as well as $LiNiO_2$. In the case of $LiNi_{0.9}Mn_{0.1}O_2$, it may be difference with electronic structure of $LiNiO_2$ that the relative intensity of band B is to be conspicuous. The spectrum of $LiNi_{0.9}Al_{0.1}O_2$ was almost equal electronic structure for $LiNiO_2$, though the features in which all of the spectra were shifting to the high energy side were recognized. It has been reported that the selectivity for OCM reaction over $LiNi_{0.9}Ti_{0.1}O_2$ and $LiNi_{0.9}Mn_{0.1}O_2$ improved but $LiNi_{0.9}Al_{0.1}O_2$ was remarkably being decreased, when it tries to compare the OCM activity of these samples with those of $LiNiO_2$. Comparing the electronic structures of $LiNiO_2$, $LiCoO_2$ and $LiNi_{1-x}M_xO_2$ (M = Ti, Al, Mn), several differences were found. These points should be examined in more detail by the CIS spectra over a wide excitation photon energy region.

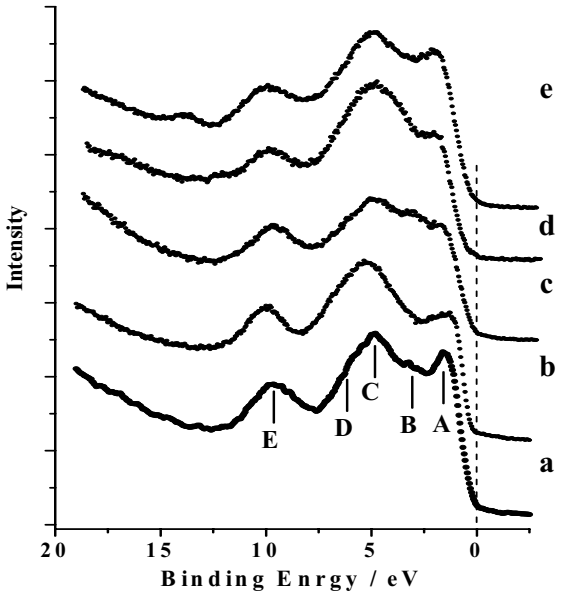

Fig. 1 The UPS spectra of a) $LiNiO_2$, b) $LiCoO_2$, c) $LiNi_{0.9}Mn_{0.1}O_2$, d) $LiNi_{0.9}Ti_{0.1}O_2$, e) $LiNi_{0.9}Al_{0.1}O_2$.

[1] T. Miyazaki *et al.*, Res. Chem. Inter. **28** (2002) 479.

[2] T. Miyazaki *et al.*, UVSOR Activity Report 2002 (2003) 197.

BL8B2

Photoemission Study of a Cu-Ga-Mg-Sc Icosahedral Phase

M. Mori[1], R. Hashimoto[1], S. Motomura[1], D. Yoshimura[2], S. Kashimoto[3], T. Ishimasa[3]
[1]*Graduate School of Information Science, Nagoya University, Chikusa, Nagoya 464-8601 Japan*
[2]*Research Center for Materials Science, Nagoya University, Chikusa, Nagoya 464-8603 Japan*
[3]*Graduate School of Engineering, Hokkaido University,Sapporo 060-8628 Japan*

Introduction

Since the discovery of an icosahedral phase (i-phase) in Al-Mn alloys by Shechtman *et al*. [1], there have been reported a large number of studies about the electronic properties of icosahedral materials in spite of remaining the arrangement of the atoms in an i-phase unclear. By intuition the pseudogap structure can be interpreted in terms of the nearly-free-electron-like energy gap inferred from the strong diffraction spots, which may be related to the stability of the i-phase.

A pseudogap-like anomaly in the DOS near E_F was directly confirmed with the photoemission study of an Al-Cu-Fe i-phase by Mori *et al*. [2]. The CIS spectra at the binding energy region between 0-2 eV show a resonant characteristic near the 3*d*-electron excitation of Fe atom in the i-phase.

Experimental and Results

The purpose is to observe the photoemission study of a new Cu-Ga-Mg-Sc (CGMS) i-phase and the Cu-Ga-Sc approximant crystal (CGS). The sample, an Cu-Ga-Mg-Sc i-phase quasicrystal, was an ingot prepared. It is well known that this is quite high quality of the quasicrystal. It was confirmed that the specimen used with this study consists of only *a new I-type i-phase* but does not contain the other phases.

Photoemission studies were performed with an angle-resolved spectrometer on beam-line BL8B2. All measurements were carried out at room temperature. The clean surface of the specimen was obtained by scraping with a diamond file in a vacuum of $2\text{-}10 * 10^{-8}$ Pa. Immediately after this proccess, the sample was transferred to the UPS experimental chamber and measured in a vacuum of $2\text{-}10 * 10^{-8}$ Pa.

The line shape near E_F is like a plateau cut off at E_F shown in Fig. 1. We have tried the fitting of the photoemission curve of the Al-Pd-Mn i-phase, using the (flat DOS) * (Gauss distribution function type resolution function. Using the fitting parameters of the Au spectrum, we could get the solid curves of lower two spectra. The middle one is well fitted with the CGS approximant crystal data. But the lower is not fitted with the CGMS quasicrystal data. This means that the CGMS quasicrystal has a pseudogap near E_F, and the CGS approximant crystal has not a pseudogap. It shows that this experimental result is well fitted as the quasicrystal has the pseudogap of width 0.4 eV and depth 0.6. This experimental result is the secondary example that the quasicrystal has the pseudogap.

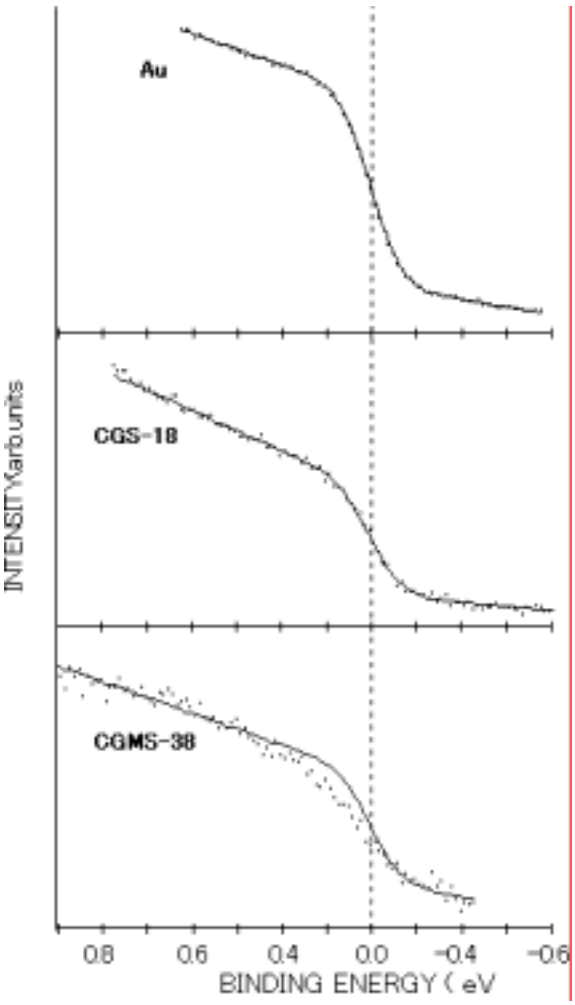

Fig. 1 Photoemission spectra near E_F measured at room temperature. Each solid curve shows the fitted curve of the DOS near E_F without pseudogap. The upper one is the spectrum of Au, and the middle is that of CGS approxmant crystal and the lower is that of CGMS i-phase quasicrystal.

[1] D. Shechtman, I. Blech, D. Gratias, J. W. Cahn, Phys. Rev. Lett. **53** (1984) 1951.
[2] M. Mori, S. Matsuo, T. Ishimasa, T. Matsuura, K. Kamiya, H. Inokuchi, T. Matsukawa, J. Phys.: Condens. Matter **3** (1991) 767; *ibid.* **4** (1992) L157.

BL8B2

Possibility of Fermi Level Control Induced by VUV-Induced Doping: UPS Study of Photodegraded PTFE Film

M. Ono[1], H. Yamane[1], H. Fukagawa[1], S. Kera[2], D. Yoshimura[3], E. Morikawa[4], K. Seki[3], N. Ueno[1]

[1]*Graduate School of Science and Technology, Chiba University, Chiba 263-8522, Japan.*
[2]*Institute for Molecular Science, Okazaki 444-8585, Japan.*
[3]*Research Center for Material Science, Nagoya University, Nagoya, 464-8602 JAPAN.*
[4]*CAMD, Louisiana State University, Baton Rouge, LA 70806, U.S.A.*

Control of Fermi level is a fundamental and extremely important technique for the development of semiconductor devices. Control of the Fermi level in the organic molecular film has been attempted by embedding metals or organic molecules. However, the method of Fermi level control is not well established. One of the most crucial problems is the difficulty to prepare a homogeneously doped film, particularly in the case of molecular doping.

The doping induced by high-energy photon irradiation is an attractive method. If photoproducts generated in the film can act as dopants, the homogeneous doping can be achieved. In addition concentration of dopants can be also controlled by the irradiation dose. As our attempt at the Fermi level control by "high-energy radiation-induced doping", the photodegradation of polytetrafluoroethylene (PTFE, -(CF_2-CF_2)$_n$-) film was studied [1]. As PTFE has a wide band gap, energy shift of the Fermi level can be easily detected.

PTFE film prepared by vacuum deposition in the UHV chamber was directly transferred to UPS measurement chamber under UHV condition. The 75-eV photon beam was utilized for both UPS measurement and photodegradation of the PTFE film. The photon dose was estimated by measuring the number of electrons emitted from the gold mesh by incidence photon.

Figure 1 shows the photodegradation effect on the UPS spectra of the PTFE film. During the VUV irradiation the UPS spectra are shifting toward low binding energy side. This shift is not due to the charge-up effect, because the shift caused by charge-up moves toward high binding energy side. In Figure 2 the binding energy positions of the four peaks are plotted against the irradiation dose. The binding energy shifts of all peaks are proportional to logarithm of the irradiation dose with identical slope. In the case of simple model which assumes only one acceptor level the energy position of the Fermi level, E_F, can be expressed by following formulae under the low-temperature approximation [2]:

$$E_F = \frac{E_a}{2} - \frac{kT}{2}\ln\left(\frac{N_a}{n_0}\right) \qquad \text{.... (1)},$$

$$n_0 = 2\left(\frac{2\pi m_h kT}{h^2}\right)^{3/2},$$

where N_a is the concentration of acceptors, E_a is the energy of acceptor level from top of the valance band and m_h is the effective mass of a hole in the valence band. It should be noted that the Fermi level position is proportional to logarithm of the concentration of the acceptor. Therefore it can be considered that the shift of UPS spectra is caused by Fermi level shift. It is expected that the radical generated by VUV light has unoccupied electronic states in the PTFE band gap. In addition the lifetime of radical is much longer (~1000 h) than the measurement time (5 h). Hence it is considered that the radical acts as acceptor upon the degradation of the PTFE film.

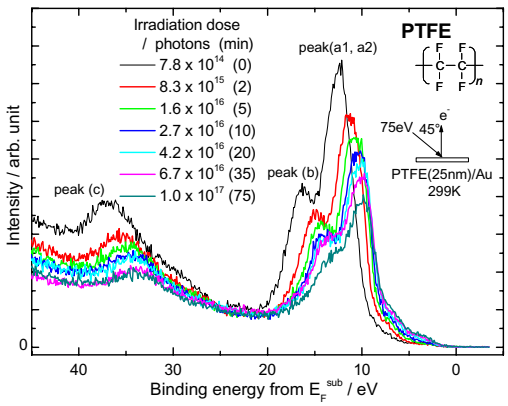

Fig. 1 VUV photodegradation effect on UPS spectra of the PTFE film.

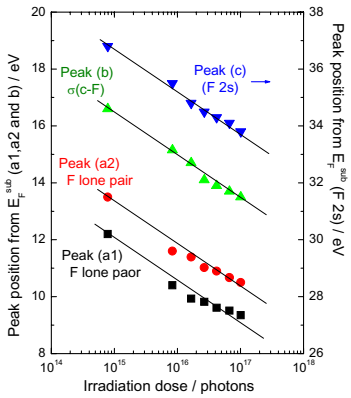

Fig. 2 The binding energy positions of the UPS peaks plotted against the irradiation dose.

[1] M. Ono *et al.*, Submitted to IPAP Conference Proceedings.
[2] C. Kittel, *Introduction to Solid State Physics,* 2nd ed. (John Wiley & Sons, New York, 1957).